



1 Validation of 10-year SAO OMI Ozone Profile (PROFOZ) 2 Product Using Ozonesonde Observations

3

4 Guanyu Huang^{1,*}, Xiong Liu¹, Kelly Chance¹, Kai Yang², Pawan K. Bhartia³, Zhaonan Cai¹,
5 Marc Allaart⁴, Bertrand Calpini⁵, Gerrie J. R. Coetzee⁶, Emilio Cuevas-Agulló⁷, Manuel
6 Cupeiro⁸, Hugo De Backer⁹, Manvendra K. Dubey¹⁰, Henry E. Fuelberg¹¹, Masatomo
7 Fujiwara¹², Sophie Godin-Beekmann¹³, Tristan J. Hall¹¹, Bryan Johnson¹⁴, Everette Joseph¹⁵,
8 Rigel Kivi¹⁶, Bogumil Kois¹⁷, Ninong Komala¹⁸, Gert König-Langlo¹⁹, Giovanni Laneve²⁰,
9 Thierry Leblanc²¹, Marion Marchand¹³, Kenneth R. Minschwaner²², Gary Morris²³, Mike J.
10 Newchurch²⁴, Shin-Ya Ogino²⁵, Nozomu Ohkawara²⁶, Ankie J. M. PETERS⁴, Françoise Posny²⁷,
11 Richard Querel²⁸, Rinus Scheele⁴, Frank J. Schmidlin³, Russell C. Schnell¹⁴, Otto Schrems¹⁹,
12 Henry Selkirk²⁹, Masato Shiotani³⁰, Pavla Skrivánková³¹, René Stübi⁵, Ghassan Taha²⁹,
13 David W. Tarasick³², Anne M. Thompson³, Valérie Thouret³³, Matt Tully³⁴, Roeland van
14 Malderen⁹, Geraint Vaughan³⁵, Holger Vömel³⁶, Peter von der Gathen³⁷, Jacquelyn C. Witte³⁸,
15 Margarita Yela³⁹

- 16 1. Harvard-Smithsonian Center for Astrophysics, Cambridge, MA, USA
17 2. Department of Atmospheric and Oceanic Science, University of Maryland, College Park,
18 Maryland, USA
19 3. NASA Goddard Space Flight Center, Greenbelt, Maryland, USA
20 4. Royal Netherlands Meteorological Institute (KNMI), De Bilt, the Netherlands
21 5. MeteoSwiss Aerological Station, Federal Office of Meteorology and Climatology
22 MeteoSwiss, Payerne, Switzerland
23 6. South African Weather Service, Pretoria, South Africa
24 7. Izana Atmospheric Research Center, Meteorological State Agency of Spain, Santa Cruz de
25 Tenerife, Spain
26 8. National Meteorological Service, Ushuaia, Tierra del Fuego, Argentina
27 9. Royal Meteorological Institute of Belgium, Brussel, Belgium
28 10. Los Alamos National Laboratory, Los Alamos, NM, USA
29 11. Earth, Ocean and Atmospheric Sciences, Florida State University, Tallahassee, FL, USA



- 30 12. Faculty of Environmental Earth Science, Hokkaido University, Sapporo, Japan
31 13. LATMOS-ISPL, Université Paris 6 Pierre-et-Marie-Curie, Paris, France
32 14. NOAA/ESRL Global Monitoring Division, Boulder, CO, USA
33 15. Atmospheric Sciences Research Center, SUNY University at Albany, Albany, NY, USA
34 16. Finnish Meteorological Institute, Helsinki, Finland
35 17. The Institute of Meteorology and Water Management, National Research Institute, Warsaw,
36 Poland
37 18. Indonesian Institute of Aeronautics and Space (LAPAN), Bandung, Indonesia
38 19. Alfred Wegener Institute for Polar and Marine Research, Bremerhaven, Germany
39 20. Earth Observation Satellite Images Applications Lab (EOSIAL), Università di Roma 'La
40 Sapienza', Rome, Italy
41 21. Jet Propulsion Laboratory, California Institute of Technology, Pasadena, CA, USA
42 22. Department of Physics, New Mexico Institute of Mining and Technology, Socorro, NM, USA
43 23. St. Edward's University, Austin, TX, USA
44 24. Department of Atmospheric Science, University of Alabama in Huntsville, Huntsville, AL,
45 USA
46 25. Department of Coupled Ocean-Atmosphere-Land Processes Research, Japan Agency for
47 Marine-Earth Science and Technology, Yokosuka, Japan
48 26. Global Environment and Marine Department, Japan Meteorological Agency, Tokyo, Japan
49 27. Université de la Réunion, Saint Denis, France
50 28. National Institute of Water and Atmospheric Research, Lauder, Central Otago, New Zealand
51 29. Universities Space Research Association, Greenbelt, MD, USA
52 30. Research Institute for Sustainable Humanosphere, Kyoto University, Kyoto, Japan
53 31. Upper Air and Surface Observation Department, Czech Hydrometeorological Institute, Praha,
54 Czech Republic
55 32. Air Quality Research Division, Environment & Climate Change Canada, Downsview, ON,
56 Canada.
57 33. Laboratoire d'Aerologie, Université de Toulouse, Toulouse, France
58 34. Observations & Infrastructure Division, Bureau of Meteorology, Melbourne, Victoria,
59 Australia



- 60 35. School of Earth, Atmosphere and Environmental Sciences, University of Manchester,
61 Manchester, U.K.
- 62 36. Earth Observing Laboratory, National Center for Atmospheric Research, Boulder, CO, USA
- 63 37. Alfred Wegener Institute, Potsdam, Germany
- 64 38. Science Systems and Applications Inc. Greenbelt, MD, USA
- 65 39. Atmospheric Research and Instrumentation Branch, National Institute for Aerospace
66 Technology (INTA), Madrid, Spain
- 67 *Correspondence to: Guanyu Huang (guanyu.huang@cfa.harvard.edu)



68 **Abstract**

69 We validate the Ozone Monitoring Instrument (OMI) ozone-profile (PROFOZ) product from
70 October 2004 through December 2014 retrieved by the Smithsonian Astrophysical Observatory
71 (SAO) algorithm against ozonesonde observations. We also evaluate the effects of OMI Row
72 anomaly (RA) on the retrieval by dividing the data set into before and after the occurrence of
73 serious OMI RA, i.e., pre-RA (2004-2008) and post-RA (2009-2014). The retrieval shows good
74 agreement with ozonesondes in the tropics and mid-latitudes and for pressure < ~50 hPa in the
75 high latitudes. It demonstrates clear improvement over the a priori down to the lower troposphere
76 in the tropics and down to an average of ~550 (300) hPa at middle (high latitudes). In the tropics
77 and mid-latitudes, the profile mean biases (MBs) are less than 6%, and the standard deviations
78 (SDs) range from 5-10% for pressure < ~50 hPa to less than 18% (27%) in the tropics (mid-
79 latitudes) for pressure > ~50 hPa after applying OMI averaging kernels to ozonesonde data. The
80 MBs of the stratospheric ozone column (SOC) are within 2% with SDs of < 5% and the MBs of
81 the tropospheric ozone column (TOC) are within 6% with SDs of 15%. In the high latitudes, the
82 profile MBs are within 10% with SDs of 5-15% for pressure < ~50 hPa, but increase to 30% with
83 SDs as great as 40% for pressure > ~50 hPa. The SOC MBs increase up to 3% with SDs as great
84 as 6% and the TOC SDs increase up to 30%. The comparison generally degrades at larger solar-
85 zenith angles (SZA) due to weaker signals and additional sources of error, leading to worse
86 performance at high latitudes and during the mid-latitude winter. Agreement also degrades with
87 increasing cloudiness for pressure > ~100 hPa and varies with cross-track position, especially with
88 large MBs and SDs at extreme off-nadir positions. In the tropics and mid-latitudes, the post-RA
89 comparison is considerably worse with larger SDs reaching 2% in the stratosphere and 8% in the
90 troposphere and up to 6% in TOC. There are systematic differences that vary with latitude
91 compared to the pre-RA comparison. The retrieval comparison demonstrates good long-term
92 stability during the pre-RA period, but exhibits a statistically significant trend of 0.14-0.7%/year
93 for pressure < ~80 hPa, 0.7 DU/year in SOC and -0.33 DU/year in TOC during the post-RA period.
94 The spatiotemporal variation of retrieval performance suggests the need to improve OMI's
95 radiometric calibration especially during the post-RA period to maintain the long-term stability
96 and reduce the latitude/season/SZA and cross-track dependence of retrieval quality.



97 **1 Introduction**

98 The Dutch-Finnish built Ozone Monitoring Instrument (OMI) on board the NASA Aura satellite
99 has been making useful measurements of trace gases including ozone and aerosols since October
100 2004. There are various retrieval algorithms to retrieve ozone profile and/or total ozone from OMI
101 data (Bak et al., 2015). The ozone profile retrieval algorithm initially developed at the Smithsonian
102 Astrophysical Observatory (Liu et al., 2005) for Global Ozone Monitoring Experiment (GOME)
103 data was adapted to OMI data (Liu et al., 2010b). Total ozone column (OC), Stratospheric Ozone
104 Column (SOC) and Tropospheric Ozone Column (TOC) can be directly derived from the retrieved
105 ozone profile with retrieval errors in in the range of a few Dobson Units (DU) (Liu et al., 2006b;
106 Liu et al., 2010a). This algorithm has been put into production in the OMI Science Investigator-
107 led Processing System (SIPS), processing the entire OMI data record with approximately one-
108 month delay. The ozone profile product titled PROFOZ is publicly available at the Aura Validation
109 Data Center (AVDC) (<http://avdc.gsfc.nasa.gov/index.php?site=2045907950>). This long-term
110 ozone profile product, with high spatial resolution and daily global coverage, constitutes a useful
111 dataset to study the spatial and temporal distribution of ozone.

112 To effectively use the retrieval dataset, it is necessary to evaluate and understand its retrieval
113 quality and long-term performance. Although validation of the ozone profile product (mostly
114 earlier versions) has been partially performed against aircraft, ozonesonde, and Microwave Limb
115 Sounder (MLS) data, these evaluations are limited to certain time periods and/or spatial region
116 and/or to only portion of the product (e.g., total ozone columns (OC) or TOC only) (Pittman et al.,
117 2009; Liu et al., 2010a; Liu et al., 2010b; Sellitto et al., 2011; Wang et al., 2011; Bak et al., 2013a;
118 Lal et al., 2013; Ziemke et al., 2014; Hayashida et al., 2015). Additionally, the quality of ozone
119 profile retrievals is very sensitive to the signal to noise ratio (SNR) of the radiance measurements
120 as well as their radiometric calibration, which may degrade over time as shown in GOME and
121 GOME-2 retrievals (Liu et al., 2007; Cai et al., 2012). Although OMI's optical degradation is
122 remarkably small to within 1-2% over the years, the SNR and the number of good spectral pixels
123 (not flagged as bad/hot pixels) have been gradually decreasing over the years due to the expected
124 CCD degradation (Claas, 2014). Furthermore, the occurrence of RA, which affects level 1b data
125 at all wavelengths for particular viewing directions or cross-track positions and likely due to
126 blocking objects in the optical path, started in June 2007 affecting a few positions. This effect



127 abruptly worsened in January 2009 affecting ~1/3 of the cross-track positions (Kroon et al., 2011).
128 The impacts of RA not only evolve with time but also vary over the duration of an orbit. Analysis
129 indicates that radiances in the UV1 channels (shorter than ~310 nm) used in our retrievals might
130 have been affected at all positions (Personal communication with S. Marchenko) and are not
131 adequately flagged for RA. Therefore, we need to evaluate the impacts of instrument degradation
132 and especially row anomaly on the temporal performance of our ozone profile product. Currently,
133 we are planning an update of the ozone profile algorithm to maintain the long-term consistency of
134 the product. The update will include empirical correction of systematic errors caused by the
135 instrument degradation and row anomaly as a function of time. Such correction also requires us to
136 evaluate the long-term retrieval quality of our product.

137 To understand retrieval quality and the resulting spatial and temporal performance of our OMI
138 product, we evaluate our data from October 2004 through December 2014 against available
139 ozonesonde and MLS observations, respectively, in two papers. This paper evaluates our ozone
140 product including both ozone profiles and stratospheric and tropospheric ozone columns using
141 ozonesonde observations with a focus on retrieval quality in the troposphere. More than 27,000
142 ozonesonde profiles from both regular ozonesonde stations and field campaigns are used in this
143 study to provide a comprehensive and global assessment of the long-term quality of our OMI ozone
144 product. This paper is followed by the validation against collocated MLS data with a focus on the
145 retrieval quality in the stratosphere (Huang et al., 2016), also submitted to this special issue).

146 This paper is organized as follows: Section 2 describes OMI retrievals and ozonesonde data. The
147 validation methodology is introduced in Section 3. Section 4 presents results, analysis and
148 discussions regarding the OMI and ozonesonde comparisons. Section 5 summarizes and concludes
149 this study.

150 **2 OMI and Ozonesonde Datasets**

151 **2.1 OMI and OMI Ozone Profile Retrievals**

152 OMI is a Dutch-Finnish built nadir-viewing pushbroom UV/visible instrument aboard the NASA
153 Earth Observing System (EOS) Aura satellite that was launched into a sun-synchronous orbit in
154 July 2004. It measures backscattered radiances in three channels covering the 270-500 nm



155 wavelength range (UV1: 270-310 nm, UV2: 310-365 nm, visible: 350-500 nm) at spectral
156 resolutions of 0.42-0.63 nm (Levelt et al., 2006). Measurements across the track are binned to 60
157 positions for UV2 and visible channels, 30 positions for the UV1 channels due to the weaker
158 signals. This results in daily global coverage with a nadir spatial resolution of 13 km × 24 km
159 (along × across track) for UV2 and visible channels, and 13 km × 48 km for the UV1 channel.

160 The SAO OMI ozone profile algorithm was adapted from the GOME ozone profile algorithm (Liu
161 et al., 2005) to OMI and was initially described in detail in Liu et al. (2010b). Profiles of partial
162 ozone columns are retrieved at 24 layers, ~2.5 km for each layer, from the surface to ~60 km using
163 OMI radiance spectra in the spectral region 270-330 nm with the optimal estimation technique. In
164 addition to the OC, SOC and TOC can be directly derived from the retrieved ozone profile with
165 the use of tropopause from the daily National Center for Environmental Protection (NCEP)
166 reanalysis data. The retrievals are constrained with month- and latitude-dependent climatological
167 a priori profiles derived from 15-year ozonesonde and SAGE/MLS data (McPeters et al., 2007)
168 with considerations of OMI random-noise errors. OMI radiances are pre-calibrated based on two
169 days of average radiance differences in the tropics between OMI observations and simulations
170 with zonal mean MLS data for pressure less than 215 hPa and climatological ozone profile for
171 pressure greater than 215 hPa. This “soft calibration” varies with wavelength and cross-track
172 positions but does not depend on space and time.

173 The updated algorithm of our SAO OMI ozone product was briefly described in Kim et al. (2013).
174 The radiative transfer calculations have been improved through the convolution of simulated
175 radiance spectra at high resolutions rather than effective cross sections, which is done by
176 interpolation from calculation at selected wavelengths assisted by weighting function. In addition,
177 four spatial pixels along the track are coadded to speed up production processes at a nadir spatial
178 resolution of 52 km × 48 km. Meanwhile, minimum measurement errors of 0.4% and 0.2% are
179 imposed in the spectral ranges 270-300 nm and 300-330 nm, respectively, to stabilize the
180 retrievals. The use of floor errors typically reduces the Degree of Freedom for Signals (DFS) and
181 increases retrieval errors. Compared to the initial retrievals, the average total, stratospheric, and
182 tropospheric DFS decrease by 0.49, 0.27, and 0.22, respectively, and the mean retrieval errors in
183 OC, SOC, and TOC increase by 0.6, 0.5, and 1.2 DU, respectively. The corresponding changes to
184 the retrievals are generally within retrieval uncertainties except for a systematic increase in



185 tropospheric ozone at SZA larger than $\sim 75^\circ$, where the TOC increases to ~ 12 DU. Validation
186 against ozonesonde data indicates that this TOC increase at large SZA makes the retrieval worse.
187 Therefore retrieved tropospheric ozone at such large SZA should not be used, but the retrieved
188 total ozone still shows good quality (Bak et al., 2015).

189 For current products, retrievals contain ~ 5.5 - 7.4 DFS, with 4.6-7.3 in the stratosphere and 0-1.2 in
190 the troposphere. Vertical resolution varies generally from 7–11 km in the stratosphere to 10–14
191 km in the troposphere, when there is adequate retrieval sensitivity to the tropospheric ozone.
192 Retrieval random-noise errors (i.e., precisions) typically range from 0.6–2.5 % in the middle
193 stratosphere to approximately 12% in the lower stratosphere and troposphere. The solution errors,
194 dominated by smoothing errors, vary generally from 1-7% in the middle stratosphere to 7-38% in
195 the troposphere. The solution errors in the integrated OC, SOC, and TOC are typically in the few
196 DU range. Errors caused by the forward model and forward model parameter assumptions are
197 generally much smaller than the smoothing error (Liu et al., 2005). The main sources of these
198 errors include systematic errors in temperature and cloud-top pressure. Systematic measurement
199 errors are the most difficult to estimate, mostly due to lack of full understanding of the OMI
200 instrument calibration.

201 Certain cross track positions in OMI data have been affected by RA since June 2007 (Kroon et al.,
202 2011). Loose thermal insulating material in front of the instrument's entrance slit is believed to
203 block and scatter light, causing measurement error. The anomaly affects radiance measurements
204 at all wavelengths for specific cross-track viewing directions that are imaged to CCD rows.
205 Initially, the anomaly only affected a few rows. But since January 2009, the anomaly has spread
206 to other rows and shifted with time. The RA also shows slight differences among different spectral
207 channels, and varies during the duration of an orbit. Pixels affected by the RA are flagged in the
208 level 1b data. The science team suggested that they are not be used in research. For data before
209 2009, the RA flagging is not applied in the processing. Pixels seriously affected by RA will
210 typically show enhanced fitting residuals. The algorithm was updated to use RA flagging in the
211 UV1 channel and was used to process the data starting from 2009. If a pixel is flagged as a row
212 anomaly then it is subsequently not retrieved to speed up the processing except that the cross-track
213 position 24 is still retrieved due to reasonably good fitting. It should be noted that the retrieval
214 quality of those non-flagged pixels may still be affected by the RA, because of the different RA



215 flagging in the UV1 and UV2, the lack of RA flagging before 2009 and inadequacy of the RA
216 flagging.

217 To screen out OMI profiles for validation, we only use OMI ozone profiles meeting the following
218 criteria based on three filtering parameters: 1) nearly clear-sky scenes with effective cloud fraction
219 less than 0.3; 2) cross track positions between 4 and 27 due to relatively worse quality and much
220 larger footprint size for these greater off-nadir positions; 3) SZA should be less than 75° due to
221 very limited retrieval sensitivity to tropospheric ozone and the aforementioned positive biases. We
222 will use all OMI pixels of each filtering parameter when evaluating retrieval quality as a function
223 of that specific parameter. The fitting quality of each retrieval is shown in the fitting RMS (root
224 mean square of the fitting residuals relative to the assumed measurement errors). The mean fitting
225 RMS including both UV1 and UV2 channels has been increasing with time as shown in Figure 1.
226 This is primarily due to the increase of fitting residuals in UV1 caused by the instrument
227 degradation and RA since the fitting residuals of UV2 only slightly increase with time. As
228 aforementioned, the retrieval information of stratospheric and tropospheric ozone mainly comes
229 from UV1 and UV2, respectively. Consequently, retrievals in the troposphere, the focus of this
230 paper, are less impacted by the increasing fitting RMS. However, to apply consistent filtering in
231 validation against both ozonesonde in this study and MLS data in the companion paper (Huang et
232 al., 2016, submitted to the same special issue), we set the RMS threshold based on the overall
233 fitting RMS and select retrievals with fitting RMS smaller than the sum of monthly mean RMS
234 and its 2σ (i.e., Standard Deviations (SDs) of fitting RMS).

235 **2.2 Ozonesondes**

236 The balloon-borne ozonesonde is a well-established technique to observe the ozone profile from
237 the surface to ~ 35 km with vertical resolution of ~ 100 - 150 m and approximately 3-5% precision
238 and 5-10% accuracy (Komhyr, 1986; Komhyr et al., 1995; Johnson, 2002; Smit et al., 2007;
239 Deshler et al., 2008). Ozonesonde data have been widely used in the studies of stratospheric ozone,
240 climate change, tropospheric ozone and air quality, as well as the validation of satellite
241 observations (Kivi et al., 2007; Wang et al., 2011; Huang et al., 2015; Thompson et al., 2015).
242 However, the accuracy of ozonesonde observations depends on data processing technique, sensor
243 solution, and instrument type and other factors. Consequently, station-to-station biases may occur



244 in ozonesonde measurements and could be as great as 10% (Thompson et al., 2007c; Worden et
245 al., 2007).

246 A decade (2004-2014) of global ozonesonde data with locations shown in Figure 2, are utilized in
247 this study to validate our OMI ozone profile product. Most of our ozonesonde data were obtained
248 from the Aura Validation Data Center (AVDC) archive. It contains routine launches from
249 ozonesonde stations, mostly weekly and occasionally 2-3 times a week at some stations. It also
250 collects launches from field campaigns, for instance, IONS 06 (INTEX-B Ozone Network Study
251 2006), ARCIONS (Arctic Intensive Ozonesonde Network Study)
252 (<http://croc.gsfc.nasa.gov/arcions/>) (Thompson et al., 2008; Tarasick et al., 2010). Data not
253 available at AVDC are obtained from other archives such as the World Ozone and Ultraviolet
254 Radiation Data Center (WOUDC) (<http://woudc.org/>), the Southern Hemisphere Additional
255 Ozonesondes (SHADOZ) (Thompson et al., 2007a; Thompson et al., 2007b), as well as archives
256 of recent field campaigns including DISCOVER-AQ (Deriving Information on Surface Conditions
257 from Column and Vertically Resolved Observations Relevant to Air Quality, [http://discover-
259 aq.larc.nasa.gov/](http://discover-
258 aq.larc.nasa.gov/)) (Thompson et al., 2015) and SEACR⁴S (Studies of Emissions and Atmospheric
260 Composition, Clouds and Climate Coupling by Regional Surveys, <https://espo.nasa.gov/home/seac4rs>) (Toon et al., 2016). Almost all of the ozonesonde data in this
261 study were obtained from electrochemical concentration cell (ECC) ozonesondes, which is based
262 on the oxidation reaction of ozone with potassium iodide (KI) in solution. The exceptions are
263 Hohenpeissenberg station in Germany that uses Brewer-Mast (BM) ozonesondes, the New Delhi,
264 Poona, and Trivandrum stations that use Indian ozonesondes, and four Japanese stations (i.e.,
265 Sapporo, Tsukuba, Naha and Syowa) that switched from KC ozonesondes to ECC ozonesondes
266 during late 2008 and early 2010. These types of ozonesondes have been reported to have larger
267 uncertainties than ECC ozonesondes (WMO, 1998; Liu et al., 2013; Hassler et al., 2014).

268 To avoid using anomalous profiles, we screen out ozonesondes that burst at pressure exceeding
269 200 hPa, ozone profiles with gaps greater than 3 km, more than 80 DU TOC or less than 100 DU
270 SOC. In the SOC comparison, we also filter measurements that do not reach 12 hPa. Some
271 ozonesonde data used in this paper (e.g. WOUDC data) are provided with a correction factor (CF)
272 derived by normalizing the integrated ozone column (appended with ozone climatology above



273 burst altitude) to the coincident total ozone column measured by a Dobson or Brewer instrument
274 to account for uncertainties in pump efficiency especially near the top of the profiles. The CF is
275 also included in our screening processes. If the CF is available, we select ozonesonde profiles with
276 the CF in the range of 0.85 to 1.15 to filter profiles that require too much correction, and apply the
277 correction. Finally, a small number of obviously erroneous profiles are visually examined and
278 rejected.

279 **3 Comparison Methodology**

280 Previous studies on the validation of satellite observations used a range of coincidence criteria.
281 Wang et al. (2011) set a 100 km radius and 3 hour time difference as coincidence criteria. Kroon
282 et al. (2011) applied coincidence criteria of $\pm 0.5^\circ$ for both latitude and longitude and 12 hours.
283 In this paper, we determine our coincident criteria based on the balance between finding most
284 coincident OMI/ozonesonde pairs to minimize differences due to spatiotemporal samplings and
285 finding a sufficient number of pairs for statistical analysis. For each screened ozonesonde profile,
286 we first select all filtered OMI data within $\pm 1^\circ$ latitude, $\pm 3^\circ$ longitude and ± 6 hours and then find
287 the nearest OMI retrieval within 100 km from the ozonesonde station to perform the validation on
288 the individual profile basis.

289 Ozonesondes have much finer vertical resolution than OMI retrievals. To account for the different
290 resolutions, ozonesonde profiles are first integrated into the corresponding OMI vertical grids and
291 then degraded to the OMI vertical resolution by using the OMI retrieval Averaging Kernels (AKs)
292 and *a priori* ozone profile based on the following equation:

$$293 \quad \hat{x} = x_a + A(x - x_a), \quad (1)$$

294 where x is the ozonesonde profile integrated into the OMI grid, \hat{x} is the retrieved ozone profile if
295 the ozonesonde is observed by OMI, A is the OMI AK matrix, and x_a is the OMI *a priori* ozone
296 profile. We refer to this retrieval as “convolved ozonesonde profile”, which is a reconstruction of
297 ozonesonde profile with OMI retrieval vertical resolution and sensitivity. Missing ozone profiles
298 above ozonesonde burst altitude are filled with OMI retrievals. The convolution process essentially
299 removes OMI smoothing errors and the impacts of *a priori* from the comparison so that
300 OMI/ozonesonde differences are mainly due to OMI/ozonesonde measurement precision,



301 spatiotemporal sampling differences and other errors. However, in the regions and altitudes where
302 OMI has low retrieval sensitivity, the comparisons can show good agreement because both the
303 retrieval and convolved ozonesonde approach the a priori profile. To overcome the limitation of
304 such a comparison, we also compare with unconvolved ozonesonde profiles since it indicates how
305 well the retrievals can represent the actual ozonesonde observations (i.e., smoothing errors are
306 included as part of retrieval errors). In addition, we also compare OMI a priori and
307 convolved/unconvolved ozonesonde profiles to indicate the retrieval improvement over the a
308 priori.

309 For consistent calculations of TOC and SOC from the OMI/ozonesonde data, the tropopause
310 pressure included in the OMI retrieval and ozonesonde burst pressure (required to be less than 12
311 hPa or ~30 km) are used as the proper boundaries. The TOC is integrated from the surface to the
312 tropopause and the SOC is integrated from the tropopause pressure to the ozonesonde burst
313 pressure.

314 The relative profile difference is calculated as $(\text{OMI} - \text{Sonde}) / \text{OMI a priori} \times 100\%$ in the present
315 comparison with ozonesonde and with MLS in the companion paper. Choosing OMI a priori rather
316 than MLS/ozonesonde is to avoid unrealistic statistics skewed by extremely small values in the
317 reference data especially in the MLS retrievals of upper troposphere and lower stratosphere ozone
318 (Liu et al., 2010a). Unlike the profile comparison, ozonesonde/OMI SOC/TOC values are used in
319 the denominator in the computation of relative difference. To exclude remaining extreme outliers
320 in the comparison statistics, values that are exceeding 3σ from the mean differences are filtered.

321 After applying the OMI/ozone filtering and coincident criteria, approximately 10,500 ozonesonde
322 profiles are used in the validation. We performed the comparison for five latitude bands: northern
323 high latitudes ($60^\circ \text{N} - 90^\circ \text{N}$), northern mid-latitudes ($30^\circ \text{N} - 60^\circ \text{N}$), tropics ($30^\circ \text{S} - 30^\circ \text{N}$), southern
324 mid-latitudes ($60^\circ \text{S} - 30^\circ \text{S}$), and southern high latitudes ($90^\circ \text{S} - 60^\circ \text{S}$) to understand the latitudinal
325 variation of the retrieval performance. We investigated the seasonal variations of the comparisons
326 mainly at northern mid-latitudes where ozone retrieval shows distinct seasonality and there are
327 adequate coincidence pairs. To investigate the RA impacts on OMI retrievals, we contrasted the
328 comparison before (2004-2008, i.e., pre-RA) and after (2009-2014, i.e., post-RA). Although we
329 filter OMI data based on cloud fraction, cross-track position, and SZA, we conduct the comparison



330 as a function of these parameters using coincidences at all latitude bands to show how these
331 parameters affect the retrieval quality. In these evaluations, the filtering of OMI data based on
332 cloud fraction, cross-track position, and SZA are switched off, respectively. Approximately 15,000
333 additional ozonesonde profiles are used in this extended evaluation. To evaluate the long-term
334 performance of our ozone profile retrievals, we analyze the monthly mean biases (MBs) of the
335 OMI/ozonesonde differences as a function of time using coincidences in the 60° S-60° N region
336 and then derive a linear trends over the entire period as well as the pre-RA and post-RA periods.

337 **4 Results and Discussions**

338 **4.1 Comparison of Ozonesonde and OMI profiles**

339 **4.1.1 Ozone Profile Differences**

340 Comparisons of ozone profiles between OMI/a priori and ozonesondes with and without applying
341 OMI AKs for the 10-year period (2004-2014) are shown in the left panels of Figure 3. The MBs
342 and SDs vary spatially with altitude and latitude. Vertically, the SD typically maximizes in the
343 upper troposphere and lower troposphere (UTLS) in all latitude bands due to significant ozone
344 variability and a priori uncertainty. Bak et al. (2013b) showed that the use of Tropopause-Based
345 (TB) ozone profile climatology with NCEP Global Forecast System (GFS) daily tropopause
346 pressure can significantly improve the a priori, and eventually reduce the retrieval uncertainty.
347 Consequently, the SDs of OMI/sonde differences in the UTLS at mid- and high-latitudes can be
348 reduced through reducing the retrieval uncertainties. Latitudinally, the agreement is better in the
349 tropics and becomes worse at higher latitudes. The patterns are generally similar in the northern
350 and southern hemispheres. The MBs between OMI and ozonesonde are within ~6% with AKs and
351 10% without AKs in the tropics and the middle latitudes. Large changes in the biases between with
352 and without AKs occur in the tropical troposphere where the bias differences reach 10%. The MBs
353 increase to 20-30% at high latitudes consistently with large oscillation from ~-20-30% at ~300 hPa
354 to +20% near the surface both with and without the application of AKs. At pressure < 50 hPa, the
355 SDs for comparisons with OMI AKs are typically 5-10% at all latitudes except for the 90° S-60°
356 S region. For pressure > 50 hPa, the SDs are within 18% and 27% in the tropics and middle-



357 latitudes, respectively, but increase to 40% at higher latitudes. The SDs for comparison without
358 applying OMI AKs, i.e., including OMI smoothing errors in the OMI/ozonesonde differences,
359 typically increase up to 5% for pressure < 50 hPa, but increase up to 15-20% for pressure > ~50hPa.
360 The smoothing errors derived from root square differences of the MBs with and without OMI AKs
361 are generally consistent with the retrieval estimate from the optimal estimation.

362 The improvements of OMI over the climatological (a priori) profiles can be reflected in the
363 reduction of MBs and SDs in the comparisons between ozonesondes and OMI retrievals, and
364 between ozonesondes and a priori. The retrieval improvements in the MBs are clearly shown in
365 the tropics and at ~ 100 hPa pressure in the middle latitudes. At high latitudes, the MBs and
366 corresponding oscillations in the troposphere are much larger than these in the a priori comparison,
367 suggesting that these large biases are mainly caused by other systematic measurements errors at
368 high latitudes (larger SZAs and thus weaker signals). As can be seen from the reduction of SDs,
369 OMI retrievals show clear improvements over the a priori at pressure < 300 hPa. For pressure >
370 300 hPa, the retrieval improvements vary with latitudes. There are consistent retrieval
371 improvements throughout the surface - 300hPa layer in the tropics and only the 550 - 300 hPa
372 layer at middle latitude, while there is no retrieval improvement over the a priori for > 300 hPa at
373 high latitudes. The failure to improve the retrieval over a priori in part of the troposphere at middle
374 and high latitudes is caused by several factors. They are the inherent reduction in retrieval
375 sensitivity to lower altitudes at larger SZAs as a result of reduced photon penetration into the
376 atmosphere, unrealized retrieval sensitivity arising from retrieval interferences with other
377 parameters (e.g., surface albedo) as discussed in Liu et al. (2010b) and the use of floor-noise of
378 0.2% that underestimate the actual OMI measurement SNR. In addition, the a priori ozone error
379 in the climatology is quite small since the SDs of the differences between the a priori and
380 ozonesonde without AKs are typically less than 20% in the lower troposphere for middle and high
381 latitudes, which also makes it more difficult to improve over the a priori comparison.

382 The right column of Figure 3 shows the comparisons between OMI retrievals and ozonesondes
383 convolved with OMI AKs in the pre-RA and post-RA periods, respectively. In the tropics and mid-
384 latitudes, the pre-RA comparison is better than the post-RA comparison, with SDs smaller by up
385 to ~8% at most altitudes especially in the troposphere. The pre-RA comparison also shows smaller
386 biases near ~300 hPa at middle latitudes while the post-RA comparison exhibits negative biases



387 reaching 8-12%. At high latitudes, the pre-RA period does not show persistent improvement
388 during the post-RA period. The pre-RA comparison shows slightly smaller SDs at most altitudes
389 and smaller negative biases by 10% around 300 hPa in the northern high latitudes, and smaller
390 positive biases by 20% near the surface in the southern high latitudes. The worse results during
391 the post-RA period are caused by increasingly noisy OMI measurements with smaller SNR and
392 the additional radiometric biases made by the RA, which vary with space and time. The smaller
393 SDs at some altitudes of high latitudes may reflect a combination of ozone variation, uneven
394 distribution of ozonesondes with varying uncertainty at different stations, and cancellation of
395 radiometric errors by the RA.

396 As seen from the number of OMI/ozonesonde coincidences shown in Figure 3, the northern mid-
397 latitudes and the tropics have sufficient coincidences to validate the retrievals as a function of
398 season. In the tropics, the retrieval comparison does exhibit little seasonality as expected (not
399 shown). Figure 4 shows the comparison similar to Figure 3(c) for each individual season at
400 northern middle latitudes. The comparison results are clearly season-dependent with best
401 agreement in the summer (except for the MBs) and the worst agreement in the winter. This
402 indicates the general best retrieval sensitivity to lower tropospheric ozone during the summer as a
403 result of small SZAs and stronger signals and worst retrieval sensitivity during the winter as a
404 result of large SZAs and weaker signals. The MBs for with and without AKs at 300 hPa vary from
405 ~12% in the winter to -10% in the summer. The overall MBs are the smallest during the spring,
406 within 6%; but the MBs at pressure < 50 hPa are the best during the summer. The maximum SDs
407 vary from 31% in the winter to 20% in the summer. Also, the retrieval in the summer shows the
408 most improvements over the a priori in the lower troposphere at all tropospheric layers except for
409 the bottom layer, while the retrievals during other seasons show the improvement over a priori
410 only above the lowermost two/three layers. The seasonal variation of retrieval quality is partially
411 caused by the seasonal variations of the retrieval sensitivity and ozone variability. Bak et al.
412 (2013b) showed that the use of TB ozone climatology with daily NCEP GFS tropopause pressure
413 can significantly reduce the seasonal dependence of the comparison with ozonesondes. In addition,
414 radiometric calibration errors such as those caused by stray light and RA also contribute to the
415 seasonal variation of retrieval quality.



416 **4.1.2 Solar Zenith Angle Dependence**

417 The SZA of low earth orbit (LEO) satellite observation varies latitudinally and seasonally;
418 therefore the SZA dependence of the retrieval can cause latitudinal and seasonal dependent
419 retrieval biases. SZA is one of the main drivers that affect retrieval sensitivity especially to
420 tropospheric ozone. At large SZA, the measured backscattered signal becomes weak due to weak
421 incoming signal and long path length; the retrieval sensitivity to the tropospheric ozone decreases
422 due to reduced photon penetration to the troposphere. In addition, measurements are subject to
423 relatively larger radiometric errors such as those from stray light and as a result of weaker signal,
424 and radiative transfer calculations can lose accuracy at larger SZA (Caudill et al., 1997).

425 Figure 5 gives the MBs and SDs of differences between OMI and ozonesondes (with OMI AKs)
426 in a function of SZAs. We can see that retrieval performance generally becomes worse at large
427 SZA. The SD typically increases with SZA especially at pressure > 300 hPa. At SZA larger than
428 75°, the SD at ~300 hPa increases to greater than ~45%. The variation of MBs with SZA is more
429 complicated. We see generally larger positive biases at larger SZA in the troposphere with > 20%
430 biases at SZA larger than 75°. The MBs near ~ 30 hPa becomes more negative at larger SZAs.
431 There is a strip of positive biases of ~10% that slightly decreases in pressure from ~50 hPa at low
432 SZA to ~10 hPa at large SZA; it might be due to some systematic radiometric biases that can affect
433 ozone at different altitudes varying with SZA. Because of the clear degradation of the retrieval
434 quality at large SZA, we set the SZA filtering threshold of 75° to filter OMI data.

435 **4.1.3 Cloud Fraction Dependence**

436 The presence of cloud affects retrieval sensitivity since clouds typically reduce sensitivity to ozone
437 below clouds and increase sensitivity to ozone above clouds. The accuracy of ozone retrievals is
438 sensitive to the uncertainties of cloud information and cloud treatment (Liu et al., 2010a; Antón
439 and Loyola, 2011; Bak et al., 2015). Our OMI ozone algorithm assumes clouds as Lambertian
440 surfaces with optical centroid cloud pressure, and partial clouds are modeled using independent
441 pixel approximation such that the overall radiance is the sum of clear and cloudy radiances
442 weighted by the effective cloud fraction. The cloud albedo is assumed to be 80% and is allowed
443 to vary (>80%) with the effective cloud fraction.



444 Figure 6 gives the influences of effective cloud fraction on the comparisons between OMI and
445 ozonesonde observations convolved with OMI AKs. The MBs and SDs do not change much with
446 cloud fraction for pressure < 100 hPa, and typically increase with the increase of cloud fraction for
447 pressure > 100 hPa. The MBs at pressure > 100 hPa, especially greater~300 hPa, increase to more
448 than 10% with cloud fraction greater than ~0.3. This indicates that the cloud fractions have small
449 impacts on the stratospheric retrievals but large impacts on the tropospheric retrievals as expected.
450 Some of the variation with cloud fraction such as negative biases near ~300 hPa at cloud fraction
451 of ~0.4 and the decreases of positive biases at ~ 50 hPa for cloud fraction greater than ~0.8 may
452 be partially related to the uncertainties of the cloud parameters. The chosen filtering threshold of
453 0.3 in cloud fraction is a tradeoff between validating OMI data with adequate retrieval sensitivity
454 to tropospheric ozone and finding adequate number of OMI/ozonesonde coincidences.

455 **4.1.4 Cross-Track Position Dependence**

456 The OMI swath is divided into 30 cross-track pixels at the UV1 spatial resolution of our product.
457 Each cross-track position is measured by a different part of the CCD detector, i.e., essentially a
458 different instrument. Radiometric calibration coefficients of the instrument are characterized
459 during pre-launch only at selected CCD column pixels and then interpolated to other columns,
460 causing variation in the radiometric calibration performance across the CCD detector. This in turn
461 causes cross-track dependent biases in the calibrated radiance (Liu et al., 2010b), which therefore
462 causes striping in almost all the OMI data products if no de-striping procedure is applied. Our
463 retrieval algorithm has included a first-order empirical correction independent of space and time
464 to remove the cross-track variability (Liu et al., 2010b). However, residual dependence on cross-
465 track position remains and the radiometric calibration at different position can degrade differently
466 with time (e.g., the RA impact). In addition, the viewing zenith angle ranges from ~0° to ~70° and
467 the footprint area increases by approximately an order of magnitude from nadir to the first/last
468 position. So the varying viewing zenith angle causes the variation of retrieval sensitivities and
469 atmospheric variabilities within varying footprint areas may also cause additional cross-track
470 dependence in the retrieval performance.

471 Figure 7 provides the MBs and SDs of the differences between OMI and ozonesonde convolved
472 with OMI AKs as a function of cross-track position for pre-RA and post-RA periods, respectively.



473 It clearly exhibits cross-track dependence especially with large positive/negative MBs and large
474 SDs at the first/last several extreme off-nadir positions. This is why we select cross-track positions
475 of 4-27 in the validation to avoid positions with large biases. The enhanced biases/SDs at positions
476 24 (RA flagging not applied) and 27 (flagged as RA in UV2 since June 25, 2007 but not
477 flagged/applied in UV1) are due to the RA impact during the post-RA period. Cross-track positions
478 1-10 show consistent bias patterns with negative biases in ~300- 50 hPa layer and positive biases
479 in ~surface – 300 hPa layer, and large standard deviation around ~ 300 hPa although the magnitude
480 decreases with increasing cross-track position. This pattern occurs during both pre-RA and post-
481 RA periods although the values are larger during the post-RA period. For other cross-track
482 positions, the variation is relatively smaller but we can still see small striping patterns.

483 **4.2 Comparison of Partial Ozone Columns**

484 We investigate and validate OMI partial ozone columns, including SOCs, TOCs, and surface-550
485 hPa and surface-750 hPa ozone columns in this section. We define the lowermost one and two
486 layer as surface-750 hPa and surface-550 hPa in this paper, respectively, for conveniences.
487 Similarly, we also analyze the validation results of SOCs and TOCs during pre-RA and post-RA,
488 respectively, to test the impacts of RA on OMI partial ozone columns. In addition, we validate
489 ozone columns from the surface to ~550 hPa (bottom two layers) and ~ 750 hPa (bottom one layer)
490 against ozonesonde observations in the tropics and mid-latitude summer where there is better
491 retrieval sensitivity to these quantities.

492 **4.2.1 Comparison of Stratospheric Ozone Columns (SOCs)**

493 The left column of Figure 8 shows the MBs and SDs of the comparisons of OMI and ozonesonde
494 SOCs for each of the five latitude bands during 2004-2014. In all regions, the OMI SOCs have
495 excellent agreement with ozonesonde SOCs regardless of whether ozonesonde data are convolved
496 with OMI AKs. The application of OMI AKs to ozonesonde SOCs only slightly improves the
497 comparison statistics. The MBs with OMI AKs are within 1.8% except for a negative bias of 3%
498 at northern high latitudes, while the SDs are within 5.1% except for 5.7% at high latitudes. The
499 correlation coefficient is greater than 0.95 except for 0.90 in the tropics due to the smaller SOC
500 range. The SDs are typically larger than the comparisons with MLS data (Liu et al., 2010a) due to



501 worse coincidence criteria, relatively larger uncertainty in the ozonesonde stratospheric ozone
502 columns compared to MLS data, and different altitude ranges of integration.

503 The middle and right columns of Figure 8 show comparison results during the pre-RA and post-
504 RA periods, respectively. The comparison is typically better during the pre-RA with SDs smaller
505 by 0.2-0.6% and larger correlation coefficients although the MBs are generally smaller during the
506 post-RA period. One exception is at southern high-latitudes where the post-RA comparison
507 statistics are significantly better except for the MB, consistent with Figure 3, likely due to a
508 combination of ozone variation between these two periods, uneven distribution of ozonesondes at
509 different stations, and cancellation of various calibration errors.

510 **4.2.2 Comparison of Partial Ozone Columns in the Troposphere**

511 The left column of Figure 9 shows the comparison of OMI and ozonesonde (with and without OMI
512 AKs) TOCs for each of the five latitude bands during 2004-2014. Without applying OMI AKs, the
513 MBs are within 1-3% except for 9% at northern high latitudes; The SDs are within 20% in the
514 tropics and mid-latitudes and increase to ~30-40% at high-latitudes. The correlation coefficient
515 ranges from 0.83 in the tropics to ~0.7 at middle latitudes, and 0.5-0.6 at high-latitudes. The linear
516 regression slopes are in the range 0.6-0.8 typically smaller at high latitudes due to reduced retrieval
517 sensitivity to the lower troposphere. After applying the OMI AKs to ozonesonde data to remove
518 smoothing errors, we see significant improvement in the comparison statistics except for MBs,
519 which are within 6% at all latitudes. The SDs are reduced to within 15% in the tropics and middle
520 latitudes and ~30% (5.5-8.1 DU) at high latitudes; the correlation improves by 0.04-0.12 and the
521 slope significantly increases by 0.12-0.23 to the range 0.8-1.0 at different latitude bands due to
522 accounting for inadequate retrieval sensitivity to the lower and middle troposphere.

523 The middle and right columns of Figure 9 show comparisons during pre-RA and post-RA,
524 respectively. The comparison between OMI and ozonesondes with OMI AKs TOCs during the
525 pre-RA period is significantly better than these during the post-RA period in the tropics and mid-
526 latitudes with SDs smaller by 3.4-5.5% and greater correlation. The MBs during the post-RA
527 period is smaller by ~2 DU at mid-latitudes, but larger by ~1 DU in the tropics. However, the post-
528 RA comparison is similar to the pre-RA comparison at northern high-latitudes and is even better
529 at southern high latitudes probably due to the aforementioned ozonesonde issues.



530 Figure 10 shows examples of time series when comparing individual OMI and ozonesondes (with
531 OMI AKs) TOCs and their corresponding differences at six selected stations, one for each latitude
532 region of 90° N-60° N, 60° N-30° N, 30° N-0°, 0°-30° S, 30° S-60° S and 60° S-90° S. OMI TOC
533 shows good agreement with ozonesondes at these stations with overall MBs ≤ 3 DU and SDs less
534 than 5.1 DU. The comparison is also good even in the high latitude regions partially because the
535 Summit and Neymayer stations only have ozonesonde launches during local summer. Seasonal
536 dependent biases are clearly seen at Payerne, and bias trends can be seen at several stations with
537 positive trends at Summit and Neumayer and a negative trend at Naha. In the pre-RA and post-RA
538 periods, the MBs are typically within 2 DU and the SDs are typically smaller during the pre-RA
539 period except for Naha. The better comparison (both mean bias and standard deviation) during the
540 post-RA period at Naha is likely due to the switch to ECC ozonesondes beginning on November
541 13, 2008 from KC ozonesonde that have greater uncertainty (WMO, 1998).

542 Figure 2 also shows the MBs and SDs of the TOC differences between OMI and ozonesonde
543 convolved with OMI AKs at each station/location where there are at least 10 coincident
544 OMI/ozonesonde pairs. OMI data generally exhibit good agreement with ozonesondes at most of
545 the stations, with MBs of ≤ 3 DU and SDs of ≤ 6 DU. In the tropics (30° S-30° N), very large SDs
546 (>11 DU) occur at the two Indian stations (New Delhi, and Trivandrum). The large bias of >6 DU
547 at New Delhi is likely associated with the large uncertainties of the Indian ozonesonde data. Hilo
548 has large biases of ~ 4.5 DU with 3.2 and 6.2 DU for pre-RA and post-RA, respectively. Java also
549 has a large bias of ~ 5 DU but shows no much difference between pre-RA and post-RA. Consistent
550 $\sim 2\%$ and $\sim 5\%$ underestimates of OC by ozonesondes compared to OMI total ozone are found in
551 Hilo and Java, respectively (Thompson et al., 2012). These OC underestimates may partly explain
552 the large TOC biases in Hilo and Java. However, the reason for underestimates of ozonesonde-
553 derived OC is unknown. In the middle latitudes, noticeably large SDs and/or biases occur at a few
554 stations such as Churchill, Sable Islands, Hohenpeissenberg, and Parah. Three Japanese stations,
555 Sapporo, Tateno, and Naha, exhibit relatively large biases of 2-3 DU and even larger biases before
556 switching from KC to ECC sondes. Almost half of the 11 northern high latitude stations (60° N-
557 90° N) and two of the 6 southern high-latitude stations have large SDs/biases. In addition to
558 retrieval biases from the OMI data, some of the large biases or SDs might be partially related to
559 ozonesonde type with different biases and uncertainties due to different types (e.g., Indian sonde



560 stations, Brewer-Mast ozonesonde at Hohenpeissenberg, three KC sonde stations), manufacturers
561 (e.g., SP vs. ENSCI for ECC sonde), sensor solution or related to individual sonde operations,
562 which was shown in the validation of GOME ozone profile retrievals (Liu et al., 2006a).

563 Figure 11 shows the comparison for each season at northern mid-latitudes. Consistent with profile
564 comparison, the TOC comparison is season-dependent. When applying OMI AKs, the mean bias
565 varies from 3 DU in winter to -1.5 DU in summer. The SDs are within 6.8 DU with the smallest
566 value during fall due to less ozone variability. The regression slopes are very close, within 0.04
567 around 0.67. The retrieval sensitivity is smallest during the summer as seen from the greatest
568 correlation and slope and relatively small standard deviation, and is the worst during the winter.
569 With OMI AKs applied to ozonesonde profiles, the MBs only slightly change (varying from 3.5
570 DU to -1.3 DU), but the SDs are significantly reduced to within 5.2 DU, the slopes significantly
571 increase by ~0.2 to 0.8-1.0, and the correlation improves significantly during the winter and spring.

572 Figure 12 compares the surface~550 hPa and surface~750 hPa ozone columns with ozonesonde
573 data in the middle latitudes during summer and the tropics. Compared to the TOC comparisons in
574 Figure 9 and Figure 11, the comparisons of these lower tropospheric ozone columns exhibit smaller
575 regression slopes and correlations that are a result of reduced retrieval sensitivity. In the tropics,
576 the slopes decrease from 0.78 in TOC to 0.65 in the surface~550 hPa ozone column and ~0.50 in
577 the surface~750 hPa column, with corresponding correlation from 0.83 to 0.74 in the surface~550
578 hPa column, and 0.66 in the surface~750 hPa column. This indicates that the retrievals in the
579 surface~550 hPa/750 hPa can capture ~65%/50% of the actual ozone change from the a priori.
580 During the middle latitude summer, the slope decreases from 0.71 in the TOC comparisons to 0.42
581 in the surface~550 hPa comparisons and 0.32 in the surface~750 hPa comparisons, with
582 corresponding correlation coefficients from 0.74 to 0.5 and 0.46. Thus, the retrievals in the
583 surface~550 hPa and ~750 hPa only capture ~40%/30% of the actual ozone change from the a
584 priori. The MBs are generally small within 0.5 DU (5%) with SDs of ~3.6 DU (20-28%) in the
585 surface~550 hPa ozone column and ~2.5 DU (25-36%) in the surface~750 hPa ozone column.
586 After applying OMI AKs to account for inadequate retrieval sensitivity and removing smoothing
587 errors, the slope significantly increases to approach 1 (as expected). SDs are reduced to ~10% in
588 the middle latitudes and ~15% in the tropics.



589 4.3 Evaluation of Long-term Performance

590 Previous evaluation indicated systematic differences between pre-RA and post-RA periods and
591 generally worse performance during the post-RA periods. To further illustrate the long-term
592 stability of our ozone profile product and understand the quality of OMI radiometric calibration as
593 a function of time, we analyze monthly MBs of OMI/ozonesonde differences with OMI retrieval
594 AKs in ozone profiles, SOCs, and TOCs. Due to the lack of OMI observations during some months
595 at high-latitudes, we focus the evaluation by using coincidence pairs in 60° S-60° N. Monthly MBs
596 are calculated only if there are more than 5 OMI-ozonesonde pairs in a given month. Linear
597 regression trend is on the MBs for the entire period (2004-2014) and/or for the pre-RA and post-
598 RA periods, respectively. The trend is considered statistically significant if its P value is less than
599 0.05.

600 The linear trends of monthly mean ozone biases for each OMI layer between 60° S-60° N are
601 plotted in Figure 13 for each of the three periods. During 2004-2014, marked in black, ozone biases
602 at layers above 50.25 hPa show significant positive trends of 0.06-0.17 DU/year (0.17-
603 0.52%/year), while ozone biases between 290 hPa and 110 hPa exhibit significant negative trends
604 of 0.1-0.19 DU/year (1-2%/year). The positive trends in the stratosphere are generally consistent
605 with those shown in OMI-MLS comparisons (Huang et al., 2016). In the lowermost three OMI
606 layers, ozone differences are more stable but with several large spikes during the post-RA periods
607 likely due to the RA evolution or instrument operation. The derived trends for the pre-RA period
608 are generally more flat and insignificant at all layers indicating good stability of our product as
609 well as the OMI radiometric calibration. During the post-RA period, the derived trends are positive
610 above 75 hPa with statistical significance. These positive trends in the stratosphere are generally
611 similar to those over the entire period, suggesting the dominant contribution of the post-RA period
612 to the overall trend. In the altitude range 214 – 108 hPa, the post-RA trends are also flat similar to
613 the pre-RA trends, but the values are systematically smaller during the post-RA period, causing
614 significantly negative trends over the entire period.

615 The SOC biases exhibit small positive trend of 0.14 ± 0.09 DU/year in 2004-2014 with no statistical
616 significance (Figure 14(a)). This slight positive trend is a result of trend cancellation by the positive
617 trends above 80 hPa and negative trends between 220 hPa and 80 hPa. The TOC biases reveal a



618 significant negative trend of -0.18 ± 0.05 DU/year (Figure 14(b)), mostly from layers in the upper
619 troposphere. In the pre-RA and post-RA periods, both trends of both SOC and TOC biases are
620 relatively flat during the pre-RA period, while the SOC trend in the post-RA period is 0.77 ± 0.20
621 DU/year with significance. It is noticeable that the P value of TOC trend in the post-RA period is
622 0.06.

623 The significant trends of ozone biases at different layers as well as in SOC and TOC suggest that
624 the current ozone profile product is not suitable for trend studies especially during the post-RA
625 period. The relatively flat bias trends during the pre-RA periods and statistically significant trends
626 during the post-RA period confirm that the better stability of our product during the pre-RA period
627 and more temporal variation of the retrieval performance during the post-RA period are likely
628 associated with the RA evolution. In previous sections, the validation of our retrievals revealed
629 latitudinal/seasonal/SZA and cross-track dependent biases even during the pre-RA period. This
630 indicates the need to remove signal dependent errors and the calibration inconsistency across the
631 track. To maintain the spatial consistency and long-term stability of our ozone profile product, we
632 need to further improve OMI's radiometric calibration especially during the post-RA period.
633 Preferably, the calibration improvement should be done in the level 0-1b processing. If this option
634 is not possible, we can perform soft calibration similar to Liu et al. (2010b) but derive the
635 correction as a function of time and latitude/SZA. In addition, it should be noted that the trend
636 calculation might be affected by factors such as the availability of correction factors with
637 ozonesondes (Morris et al., 2013), station-to-station variability and the uneven spatiotemporal
638 distribution of the ozonesondes, which can introduce considerable sampling biases (Liu et al.,
639 2009; Saunio et al., 2012).

640 **5 Summary and Conclusion**

641 We conducted a comprehensive evaluation of the quality of OMI ozone profile (PROFOZ)
642 products produced by the SAO algorithm, including their spatial consistency and long-term
643 performance using coincident global ozonesonde observations during the decade 2004-2014. To
644 better understand retrieval errors and sensitivity, we compared the retrieved ozone profiles and a
645 priori profile at individual layers with ozonesondes before and after being degraded to the OMI
646 vertical resolution with OMI retrieval average kernels (AKs). We also compared the integrated



647 SOC, TOC, and surface ~ 550 / ~ 750 hPa ozone columns with ozonesonde data. To understand the
648 spatial distribution of retrieval performance, the validations are grouped into five latitude ranges:
649 northern/southern high/middle latitudes, and the tropics. To investigate the impacts of the OMI
650 row anomaly (RA) on the retrievals, we contrasted the comparison before and after the occurrence
651 of major OMI RA in January 2009, i.e., pre-RA (2004-2008) and post-RA (2009-2014) periods.
652 In addition, we quantified the dependence of retrieval performance on seasonality and several key
653 parameters including solar zenith angle (SZA), cloud fraction, and cross-track position. Finally,
654 we analyzed the monthly mean variation of the mean biases (MBs) to examine the long-term
655 stability of the PROFOZ product.

656 The comparison between OMI and ozonesonde profiles varies in altitude, with maximum standard
657 deviations (SDs) in the Upper Troposphere and Lower Stratosphere (UTLS) due to significant
658 ozone variability, and varies with latitude similarly in the northern and southern hemispheres.
659 There is good agreement throughout the atmosphere in the tropics and mid-latitudes. With the
660 application of OMI AKs to ozonesonde data, the MBs are within 6%, and the SDs increase from
661 5-10% for pressure $< \sim 50$ hPa to within 18%(27%) in the tropics/mid-latitudes for pressure $> \sim 50$
662 hPa. In the high latitudes, the retrievals agree well with ozonesondes only for pressure $< \sim 50$ hPa
663 with MBs of $< 10\%$ and SDs of 5-15% for pressure $< \sim 50$ hPa, but with MBs reaching 30% and
664 SDs reaching 40% for pressure $> \sim 50$ hPa. The comparison is seasonally dependent. At northern
665 mid-latitudes, the agreement is generally best (except for MBs) in the summer, with the best
666 retrieval sensitivity and the smallest SDs as great as 20%, and the worst in the winter with the
667 worst retrieval sensitivity and the largest SDs reaching 31%. The MBs near 300 hPa vary from
668 12% in the winter to -10% in the summer. The post-RA comparison is generally worse in the
669 tropics and mid-latitudes than the pre-RA comparison, with SDs larger by up to 8% in the
670 troposphere and 2% in the stratosphere, and with larger MBs around ~ 300 hPa in the mid-latitudes.
671 But at high latitudes, the pre-RA comparison does not show persistent improvement over the post-
672 RA comparison, with smaller biases and larger SDs at some altitudes, especially at southern high
673 latitudes. The retrieval improvement over a priori can be determined from the SD reduction of the
674 retrieval comparison from the a priori comparison. The retrievals demonstrate clear improvement
675 over the a priori down to the surface in the tropics, but only down to ~ 750 hPa during mid-latitude
676 summer, ~ 550 hPa during the other seasons of mid-latitudes and ~ 300 hPa at high latitudes.



677 Retrieval performance typically becomes worse at large SZA, especially at SZA larger than 75°,
678 where the MBs in the troposphere are >20% and the SDs near ~300 hPa are > 45%. The worse
679 performance at larger SZA is due to a combination of weaker signal and greater influence by
680 radiometric calibration errors such as due to stray light, and radiative transfer calculation errors.
681 The variation of SZA is likely responsible for the majority of the retrieval dependence on latitude
682 and season. The retrieval quality for pressure > ~100 hPa degrades with increasing cloudiness in
683 terms of MBs and SDs, with MBs greater than 10% at cloud fraction > 0.3. The retrieval
684 performance also varies with cross-track position, especially with large MBs and SDs at the
685 first/last extreme off-nadir positions (e.g., 1-3 and 28-30). The dependence is stronger during the
686 post-RA period.

687 The integrated SOCs and TOCs also exhibit good agreement with ozonesondes. With the
688 convolution of OMI AKs to ozonesonde data, the SOC MBs are within 2% with SDs within ~5.1%
689 in the tropics and mid-latitudes. These statistics do not change much even without the applications
690 of OMI AKs. The comparison becomes slightly worse at high latitudes, with MBs up to 3% and
691 SDs up to 6%. The pre-RA comparison is generally better with smaller SDs of 0.2-0.6% except
692 for southern high latitudes, although with slightly larger MBs. The TOC MBs and SDs with OMI
693 AKs are within 6%, with SDs of <~15% in the tropics and mid-latitudes but reach 30% at high
694 latitudes. The pre-RA TOC comparison is also better in the tropics and mid-latitudes with SDs
695 smaller by 3.4-5.5% but worse values at southern high latitudes. The TOC comparison at northern
696 mid-latitudes varies with season, with MBs of 11%. There are worse correlation during winter
697 and MBs of -3% and best correlation in summer. The TOC comparison also shows noticeable
698 station-to-station variability in similar latitude ranges with much larger MBs and/or SDs at the two
699 Indian stations and larger MBs at several Japanese stations before they switched from KC
700 ozonesondes to ECC ozonesondes. This demonstrates the impacts of ozonesonde uncertainties
701 due to sonde types, manufacturers, sensor solution and operations. Without applying OMI AKs,
702 the TOC correlation with ozonesondes typically becomes worse at higher latitudes, ranging from
703 0.83 in the tropics to 0.5-0.6 at high latitudes. The linear regression slope is within 0.6-0.8,
704 typically smaller at higher latitudes, reflecting the smaller retrieval sensitivity down to the
705 troposphere at higher latitudes mainly resulting from larger SZA. The convolution of AKs



706 significantly improves the correlation and slope. The impact of retrieval sensitivity related to SZA
707 is also reflected in the seasonal dependence of the comparison at mid-latitudes.

708 The surface~550/750 hPa ozone columns in the tropics during mid-latitude summer compare
709 quite well with ozonesonde data, with MBs of < 5% and SDs of 20-25%/28-36% without OMI
710 AKs. The correlation and slope decrease with decreasing altitude range due to reduced retrieval
711 sensitivity down to the lower troposphere. These columns capture ~65%/50% of the actual ozone
712 change in the tropics and ~40%/30% in the troposphere. Convolving ozonesonde data with OMI
713 AKs significantly increases the slope to ~1 and reduce the SDs to 10-15%.

714 The contrast of pre-RA and post-RA comparisons indicates generally worse post-RA performance
715 with larger SDs. Linear trend analysis of the OMI/ozonesonde monthly MBs further reveals
716 additional RA impact. The temporal performance over 60° S-60° N is generally stable with no
717 statistically significant trend during the pre-RA period, but displays a statistically significant trend
718 of 0.14-0.7%/year at individual layers for pressure < ~80 hPa, 0.7 DU/year in SOC and -0.33
719 DU/year in TOC during the post-RA period. Because of these artificial trends in our product, we
720 caution against using our product for ozone trend studies.

721 This validation study demonstrates generally good retrieval performance of our ozone profile
722 product especially in the tropics and mid-latitudes during the pre-RA period. However, the
723 spatiotemporal variation of retrieval performance suggests that OMI's radiometric calibration
724 should be improved, especially during the post-RA period, including the removal of signal-
725 dependent errors, calibration inconsistency across the track and with time to maintain the long-
726 term stability and spatial consistency of our ozone profile product.

727

728 **Acknowledgements**

729 This study was supported by the NASA Atmospheric Composition: Aura Science Team
730 (NNX14AF16G) and the Smithsonian Institution. The Dutch-Finnish OMI instrument is part of
731 the NASA EOS Aura satellite payload. The OMI Project is managed by NIVR and KNMI in the
732 Netherlands. We acknowledge the OMI International Science Team for producing OMI data. We
733 also acknowledge the ozonesonde providers and their funding agencies for making ozonesonde



734 measurements, and the Aura Validation Data Center (AVDC), WOUDC, SHADOZ, DISCOVER-
735 AQ, and SEACR⁴S for archiving the ozonesonde data.

736 **References**

- 737 Antón, M., and Loyola, D.: Influence of cloud properties on satellite total ozone observations, J.
738 Geophys. Res., 116, doi: 10.1029/2010JD014780, 2011.
- 739 Bak, J., Kim, J. H., Liu, X., Chance, K., and Kim, J.: Evaluation of ozone profile and tropospheric
740 ozone retrievals from GEMS and OMI spectra, Atmos. Meas. Tech., 6, 239-249, 2013a.
- 741 Bak, J., Liu, X., Wei, J. C., Pan, L. L., Chance, K., and Kim, J. H.: Improvement of OMI ozone
742 profile retrievals in the upper troposphere and lower stratosphere by the use of a tropopause-based
743 ozone profile climatology, Atmos. Meas. Tech., 6, 2239-2254, doi: 10.5194/amt-6-2239-2013,
744 2013b.
- 745 Bak, J., Liu, X., Kim, J. H., Chance, K., and Haffner, D. P.: Validation of OMI total ozone
746 retrievals from the SAO ozone profile algorithm and three operational algorithms with Brewer
747 measurements, Atmos. Chem. Phys., 15, 667-683, doi: 10.5194/acp-15-667-2015, 2015.
- 748 Cai, Z., Liu, Y., Liu, X., Chance, K., Nowlan, C. R., Lang, R., Munro, R., and Suleiman, R.:
749 Characterization and correction of Global Ozone Monitoring Experiment 2 ultraviolet
750 measurements and application to ozone profile retrievals, J. Geophys. Res., 117, doi:
751 10.1029/2011jd017096, 2012.
- 752 Caudill, T. R., Flittner, D. E., Herman, B. M., Torres, O., and McPeters, R. D.: Evaluation of the
753 pseudo-spherical approximation for backscattered ultraviolet radiances and ozone retrieval, J.
754 Geophys. Res., 102, 3881-3890, 1997.
- 755 Claas, J.: OMI and AURA: Status, Instrument, Spacecraft and Operations, OMI Science Meeting
756 Meeting, De Bilt, the Netherlands, 2014.
- 757 Deshler, T., Mercer, J. L., Smit, H. G. J., Stubi, R., Levrat, G., Johnson, B. J., Oltmans, S. J., Kivi,
758 R., Thompson, A. M., Witte, J., Davies, J., Schmidlin, F. J., Brothers, G., and Sasaki, T.:
759 Atmospheric comparison of electrochemical cell ozonesondes from different manufacturers, and
760 with different cathode solution strengths: The Balloon Experiment on Standards for Ozonesondes,
761 J. Geophys. Res., 113, doi: 10.1029/2007JD008975, 2008.
- 762 Hassler, B., Petropavlovskikh, I., Staehelin, J., August, T., Bhartia, P. K., Clerbaux, C.,
763 Degenstein, D., Mazière, M. D., Dinelli, B. M., Dudhia, A., Dufour, G., Frith, S. M., Froidevaux,
764 L., Godin-Beekmann, S., Granville, J., Harris, N. R. P., Hoppel, K., Hubert, D., Kasai, Y., Kurylo,
765 M. J., Kyrölä, E., Lambert, J. C., Levelt, P. F., McElroy, C. T., McPeters, R. D., Munro, R.,
766 Nakajima, H., Parrish, A., Raspollini, P., Remsberg, E. E., Rosenlof, K. H., Rozanov, A., Sano,
767 T., Sasano, Y., Shiotani, M., Smit, H. G. J., Stiller, G., Tamminen, J., Tarasick, D. W., Urban, J.,
768 van der A, R. J., Veefkind, J. P., Vigouroux, C., von Clarmann, T., von Savigny, C., Walker, K.
769 A., Weber, M., Wild, J., and Zawodny, J. M.: Past changes in the vertical distribution of ozone -
770 Part 1: Measurement techniques, uncertainties and availability, Atmos. Meas. Tech., 7, 1395-1427,
771 doi: 10.5194/amt-7-1395-2014, 2014.
- 772 Hayashida, S., Liu, X., Ono, A., Yang, K., and Chance, K.: Observation of ozone enhancement in
773 the lower troposphere over East Asia from a space-borne ultraviolet spectrometer, Atmos. Chem.
774 Phys., 15, 9865-9881, doi: 10.5194/acp-15-9865-2015, 2015.



- 775 Huang, G., Newchurch, M. J., Kuang, S., Buckley, P. I., Cantrell, W., and Wang, L.: Definition
776 and determination of ozone laminae using Continuous Wavelet Transform (CWT) analysis,
777 Atmos. Environ., 104, 125-131, doi: 10.1016/j.atmosenv.2014.12.027, 2015.
- 778 Huang, G., Liu, X., and Chance, K.: Validation of 10-year (2004-2014) SAO OMI Ozone Profiles
779 and Stratospheric Ozone Columns using Aura Microwave Limb Sounder (MLS) Atmos. Chem.
780 Phys., In prep., 2016.
- 781 Johnson, B. J.: Electrochemical concentration cell (ECC) ozonesonde pump efficiency
782 measurements and tests on the sensitivity to ozone of buffered and unbuffered ECC sensor cathode
783 solutions, IEEE T. Geosci. Remote., 107, 4393, doi: 10.1029/2001jd000557, 2002.
- 784 Kim, P. S., Jacob, D. J., Liu, X., Warner, J. X., Yang, K., Chance, K., Thouret, V., and Nedelec,
785 P.: Global ozone-CO correlations from OMI and AIRS: constraints on tropospheric ozone sources,
786 Atmos. Chem. Phys., 13, 9321-9335, doi: 10.5194/acp-13-9321-2013, 2013.
- 787 Kivi, R., Kyrö, E., Turunen, T., Harris, N. R. P., von der Gathen, P., Rex, M., Andersen, S. B., and
788 Wohltmann, I.: Ozonesonde observations in the Arctic during 1989-2003: Ozone variability and
789 trends in the lower stratosphere and free troposphere, J. Geophys. Res., 112, doi:
790 10.1029/2006JD007271, 2007.
- 791 Komhyr, W. D.: Operations on handbook-Ozone measurements to 40-km altitude with model 4A
792 electrochemical concentration cell (ECC) ozonesondes, NOAA Tech. Memo. ERLARL-149 Air
793 Resour. Lab., Boulder, CO, 49 pp., 1986.
- 794 Komhyr, W. D., Connor, B. J., McDermid, I. S., McGee, T. J., Parrish, A. D., and Margitan, J. J.:
795 Comparison of STOIC 1989 ground-based lidar, microwave spectrometer, and Dobson
796 spectrophotometer Umkehr ozone profiles with ozone profiles from balloon-borne electrochemical
797 concentration cell ozonesondes, J. Geophys. Res., 100, 9273-9282, 1995.
- 798 Kroon, M., de Haan, J. F., Veefkind, J. P., Froidevaux, L., Wang, R., Kivi, R., and Hakkarainen,
799 J. J.: Validation of operational ozone profiles from the Ozone Monitoring Instrument, J. Geophys.
800 Res., 116, D18305, doi: 10.1029/2010jd015100, 2011.
- 801 Lal, S., Venkataramani, S., Srivastava, S., Gupta, S., Mallik, C., Naja, M., Sarangi, T., Acharya,
802 Y. B., and Liu, X.: Transport effects on the vertical distribution of tropospheric ozone over the
803 tropical marine regions surrounding India, J. Geophys. Res., 118, 1513-1524, 2013.
- 804 Levelt, P. F., van den Oord, G. H. J., Dobber, M. R., Malkki, A., Visser, H., de Vries, J., Stammes,
805 P., Lundell, J. O. V., and Saari, H.: The Ozone Monitoring Instrument, IEEE T. Geosci. Remote.,
806 44, 1093-1101, 2006.
- 807 Liu, G., Tarasick, D. W., Fioletov, V. E., Sioris, C. E., and Rochon, Y. J.: Ozone correlation lengths
808 and measurement uncertainties from analysis of historical ozonesonde data in North America and
809 Europe, J. Geophys. Res., 114, doi: 10.1029/2008JD010576, 2009.
- 810 Liu, G., Liu, J., Tarasick, D. W., Fioletov, V. E., Jin, J. J., Moeini, O., Liu, X., Sioris, C. E., and
811 Osman, M.: A global tropospheric ozone climatology from trajectory-mapped ozone soundings,
812 Atmos. Chem. Phys., 13, 10659-10675, doi: 10.5194/acp-13-10659-2013, 2013.
- 813 Liu, X., Chance, K., Sioris, C. E., Spurr, R. J. D., Kurosu, T. P., Martin, R. V., and Newchurch,
814 M. J.: Ozone profile and tropospheric ozone retrievals from the Global Ozone Monitoring



- 815 Experiment: Algorithm description and validation, *J. Geophys. Res.*, 110, D20307, doi:
816 10.1029/2005jd006240, 2005.
- 817 Liu, X., Chance, K., Sioris, C. E., Kurosu, T. P., and Newchurch, M. J.: Intercomparison of GOME,
818 ozonesonde, and SAGE II measurements of ozone: Demonstration of the need to homogenize
819 available ozonesonde data sets, *J. Geophys. Res.*, 111, D114305, doi: 10.1029/2005jd006718,
820 2006a.
- 821 Liu, X., Chance, K., Sioris, C. E., Kurosu, T. P., Spurr, R. J. D., Martin, R. V., Fu, T.-M., Logan,
822 J. A., Jacob, D. J., Palmer, P. I., Newchurch, M. J., Megretskaia, I. A., and Chatfield, R. B.: First
823 directly retrieved global distribution of tropospheric column ozone from GOME: Comparison with
824 the GEOS-CHEM model, *J. Geophys. Res.*, 111, doi: 10.1029/2005JD006564, 2006b.
- 825 Liu, X., Chance, K., and Kurosu, T. P.: Improved ozone profile retrievals from GOME data with
826 degradation correction in reflectance, *Atmos. Chem. Phys.*, 7, 1575-1583, 2007.
- 827 Liu, X., Bhartia, P. K., Chance, K., Froidevaux, L., Spurr, R. J. D., and Kurosu, T. P.: Validation
828 of Ozone Monitoring Instrument (OMI) ozone profiles and stratospheric ozone columns with
829 Microwave Limb Sounder (MLS) measurements, *Atmos. Chem. Phys.*, 10, 2539-2549, doi:
830 10.5194/acp-10-2539-2010, 2010a.
- 831 Liu, X., Bhartia, P. K., Chance, K., Spurr, R. J. D., and Kurosu, T. P.: Ozone profile retrievals
832 from the Ozone Monitoring Instrument, *Atmos. Chem. Phys.*, 10, 2521-2537, doi: 10.5194/acp-
833 10-2521-2010, 2010b.
- 834 McPeters, R. D., Labow, G. J., and Logan, J. A.: Ozone climatological profiles for satellite retrieval
835 algorithms, *J. Geophys. Res.*, 112, D05308, doi: 10.1029/2005jd006823, 2007.
- 836 Morris, G. A., Labow, G., Akimoto, H., Takigawa, M., Fujiwara, M., Hasebe, F., Hirokawa, J.,
837 and Koide, T.: On the use of the correction factor with Japanese ozonesonde data, *Atmos. Chem.*
838 *Phys.*, 13, 1243-1260, doi: 10.5194/acp-13-1243-2013, 2013.
- 839 Pittman, J. V., Pan, L. L., Wei, J. C., Irion, F. W., Liu, X., Maddy, E. S., Barnet, C. D., Chance,
840 K., and Gao, R.-S.: Evaluation of AIRS, IASI, and OMI ozone profile retrievals in the extratropical
841 tropopause region using in situ aircraft measurements, *J. Geophys. Res.*, 114, 24109, doi:
842 10.1029/2009jd012493, 2009.
- 843 Saunio, M., Emmons, L., Lamarque, J. F., Tilmes, S., Wespes, C., Thouret, V., and Schultz, M.:
844 Impact of sampling frequency in the analysis of tropospheric ozone observations, *Atmos. Chem.*
845 *Phys.*, 12, 6757-6773, doi: 10.5194/acp-12-6757-2012, 2012.
- 846 Sellitto, P., Bojkov, B. R., Liu, X., Chance, K., and Del Frate, F.: Tropospheric ozone column
847 retrieval at northern mid-latitudes from the Ozone Monitoring Instrument by means of a neural
848 network algorithm, *Atmospheric Measurement Techniques*, 4, 2375-2388, 2011.
- 849 Smit, H. G. J., Straeter, W., Johnson, B. J., Oltmans, S. J., Davies, J., Tarasick, D. W., Hoegger,
850 B., Stubi, R., Schmidlin, F. J., Northam, T., Thompson, A. M., Witte, J. C., Boyd, I., and Posny,
851 F.: Assessment of the performance of ECC-ozonesondes under quasi-flight conditions in the
852 environmental simulation chamber: Insights from the Juelich Ozone Sonde Intercomparison
853 Experiment (JOSIE), *J. Geophys. Res.*, 112, 19306, 2007.



- 854 Tarasick, D. W., Jin, J. J., Fioletov, V. E., Liu, G., Thompson, A. M., Oltmans, S. J., Liu, J., Sioris,
855 C. E., Liu, X., Cooper, O. R., Dann, T., and Thouret, V.: High-resolution tropospheric ozone fields
856 for INTEX and ARCTAS from IONS ozonesondes, *J. Geophys. Res.*, 115, 20301, doi: doi:
857 10.1029/2009JD012918, 2010.
- 858 Thompson, A. M., Stone, J. B., Witte, J. C., Miller, S. K., Oltmans, S. J., Kucsera, T. L., Ross, K.
859 L., Pickering, K. E., Merrill, J. T., Forbes, G., Tarasick, D. W., Joseph, E., Schmidlin, F. J.,
860 McMillan, W. W., Warner, J., Hints, E. J., and Johnson, J. E.: Intercontinental Chemical
861 Transport Experiment Ozonesonde Network Study (IONS) 2004: 2. Tropospheric ozone budgets
862 and variability over northeastern North America, *J. Geophys. Res.*, 112, doi:
863 10.1029/2006jd007670, 2007a.
- 864 Thompson, A. M., Stone, J. B., Witte, J. C., Miller, S. K., Pierce, R. B., Chatfield, R. B., Oltmans,
865 S. J., Cooper, O. R., Loucks, A. L., Taubman, B. F., Johnson, B. J., Joseph, E., Kucsera, T. L.,
866 Merrill, J. T., Morris, G. A., Hersey, S., Forbes, G., Newchurch, M. J., Schmidlin, F. J., Tarasick,
867 D. W., Thouret, V., and Cammas, J.-P.: Intercontinental Chemical Transport Experiment
868 Ozonesonde Network Study (IONS) 2004: 1. Summertime upper troposphere/lower stratosphere
869 ozone over northeastern North America, *J. Geophys. Res.*, 112, doi: 10.1029/2006jd007441,
870 2007b.
- 871 Thompson, A. M., Witte, J. C., Smit, H. G. J., Oltmans, S. J., Johnson, B. J., Kirchhoff, V. W. J.
872 H., and Schmidlin, F. J.: Southern Hemisphere Additional Ozonesondes (SHADOZ) 1998–2004
873 tropical ozone climatology: 3. Instrumentation, station-to-station variability, and evaluation with
874 simulated flight profiles, *J. Geophys. Res.*, 112, doi: 10.1029/2005jd007042, 2007c.
- 875 Thompson, A. M., Yorks, J. E., Miller, S. K., Witte, J. C., Dougherty, K. M., Morris, G. A.,
876 Baumgardner, D., Ladino, L., and Rappenglück, B.: Tropospheric ozone sources and wave activity
877 over Mexico City and Houston during MILAGRO/Intercontinental Transport Experiment
878 (INTEX-B) Ozonesonde Network Study, 2006 (IONS-06), *Atmos. Chem. Phys.*, 8, 5113-5125,
879 2008.
- 880 Thompson, A. M., Miller, S. K., Tilmes, S., Kollonige, D. W., Witte, J. C., Oltmans, S. J., Johnson,
881 B. J., Fujiwara, M., Schmidlin, F. J., Coetzee, G. J. R., Komala, N., Maata, M., bt Mohamad, M.,
882 Nguyo, J., Mutai, C., Ogino, S. Y., Da Silva, F. R., Leme, N. M. P., Posny, F., Scheele, R., Selkirk,
883 H. B., Shiotani, M., Stübi, R., Levrat, G., Calpini, B., Thouret, V., Tsuruta, H., Canossa, J. V.,
884 Vömel, H., Yonemura, S., Diaz, J. A., Tan Thanh, N. T., and Thuy Ha, H. T.: Southern Hemisphere
885 Additional Ozonesondes (SHADOZ) ozone climatology (2005-2009): Tropospheric and tropical
886 tropopause layer (TTL) profiles with comparisons to OMI-based ozone products, *J. Geophys. Res.*,
887 117, doi: 10.1029/2011jd016911, 2012.
- 888 Thompson, A. M., Stauffer, R. M., Miller, S. K., Martins, D. K., Joseph, E., Weinheimer, A. J.,
889 and Diskin, G. S.: Ozone profiles in the Baltimore-Washington region (2006-2011): satellite
890 comparisons and DISCOVER-AQ observations, *J Atmos Chem*, 72, 393-422, doi:
891 10.1007/s10874-014-9283-z, 2015.
- 892 Toon, O. B., Maring, H., Dibb, J., Ferrare, R., Jacob, D. J., Jensen, E. J., Luo, Z. J., Mace, G. G.,
893 Pan, L. L., Pfister, L., Rosenlof, K. H., Redemann, J., Reid, J. S., Singh, H. B., Thompson, A. M.,
894 Yokelson, R., Minnis, P., Chen, G., Jucks, K. W., and Pszenny, A.: Planning, implementation, and
895 scientific goals of the Studies of Emissions and Atmospheric Composition, Clouds and Climate

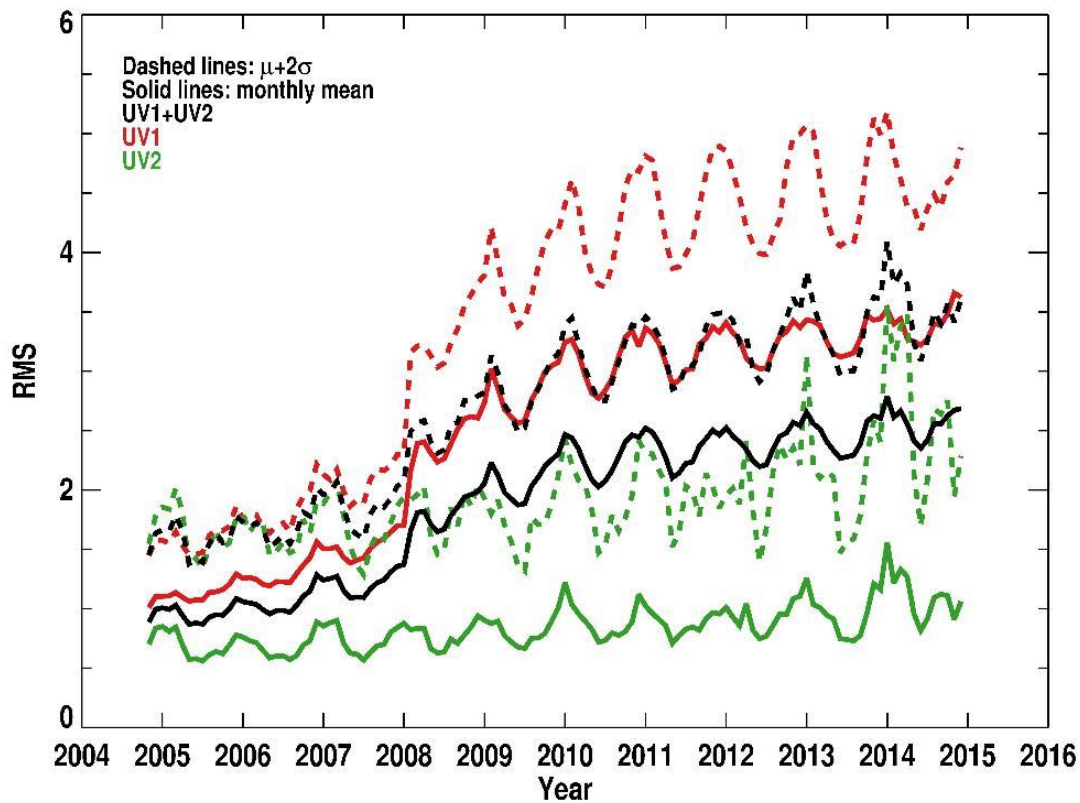


- 896 Coupling by Regional Surveys (SEAC4RS) field mission, *J. Geophys. Res.*, 121, 4967-5009, doi:
897 10.1002/2015jd024297, 2016.
- 898 Wang, L., Newchurch, M. J., Biazar, A., Liu, X., Kuang, S., Khan, M., and Chance, K.: Evaluating
899 AURA/OMI ozone profiles using ozonesonde data and EPA surface measurements for August
900 2006, *Atmos. Environ.*, 45, 5523-5530, doi: 10.1016/j.atmosenv.2011.06.012, 2011.
- 901 WMO: SPARC/IO3C/GAW Assessment of trends in the vertical distribution of ozone,
902 GenevaRep. 43, 1998.
- 903 Worden, H. M., Logan, J. A., Worden, J. R., Beer, R., Bowman, K., Clough, S. A., Eldering, A.,
904 Fisher, B. M., Gunson, M. R., Herman, R. L., Kulawik, S. S., Lampel, M. C., Luo, M.,
905 Megretskaia, I. A., Osterman, G. B., and Shephard, M. W.: Comparisons of Tropospheric Emission
906 Spectrometer (TES) ozone profiles to ozonesondes: Methods and initial results, *J. Geophys. Res.*,
907 112, doi: 10.1029/2006jd007258, 2007.
- 908 Ziemke, J. R., Olsen, M. A., Witte, J. C., Douglass, A. R., Strahan, S. E., Wargan, K., Liu, X.,
909 Schoeberl, M. R., Yang, K., Kaplan, T. B., Pawson, S., Duncan, B. N., Newman, P. A., Bhartia,
910 P. K., and Heney, M. K.: Assessment and applications of NASA ozone data products derived from
911 Aura OMI/MLS satellite measurements in context of the GMI chemical transport model, *J.*
912 *Geophys. Res.*, 119, 5671-5699, doi: 10.1002/2013jd020914, 2014.
- 913
- 914



915 **Figures and Figure Captions**

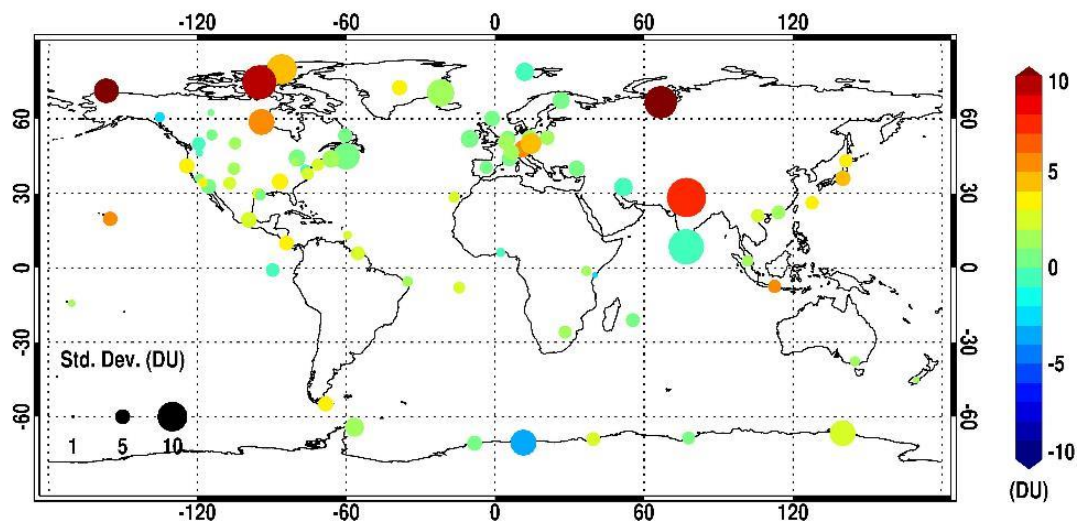
916



917

918 **Figure 1** Variation of monthly mean OMI RMS (defined as Root Mean Square of the ratio of radiance
919 residuals to assumed radiance errors). The dashed and solid lines represent respectively the monthly
920 mean RMS, and the sum of monthly mean plus its two standard deviations that is set as the RMS
921 threshold for data screening.

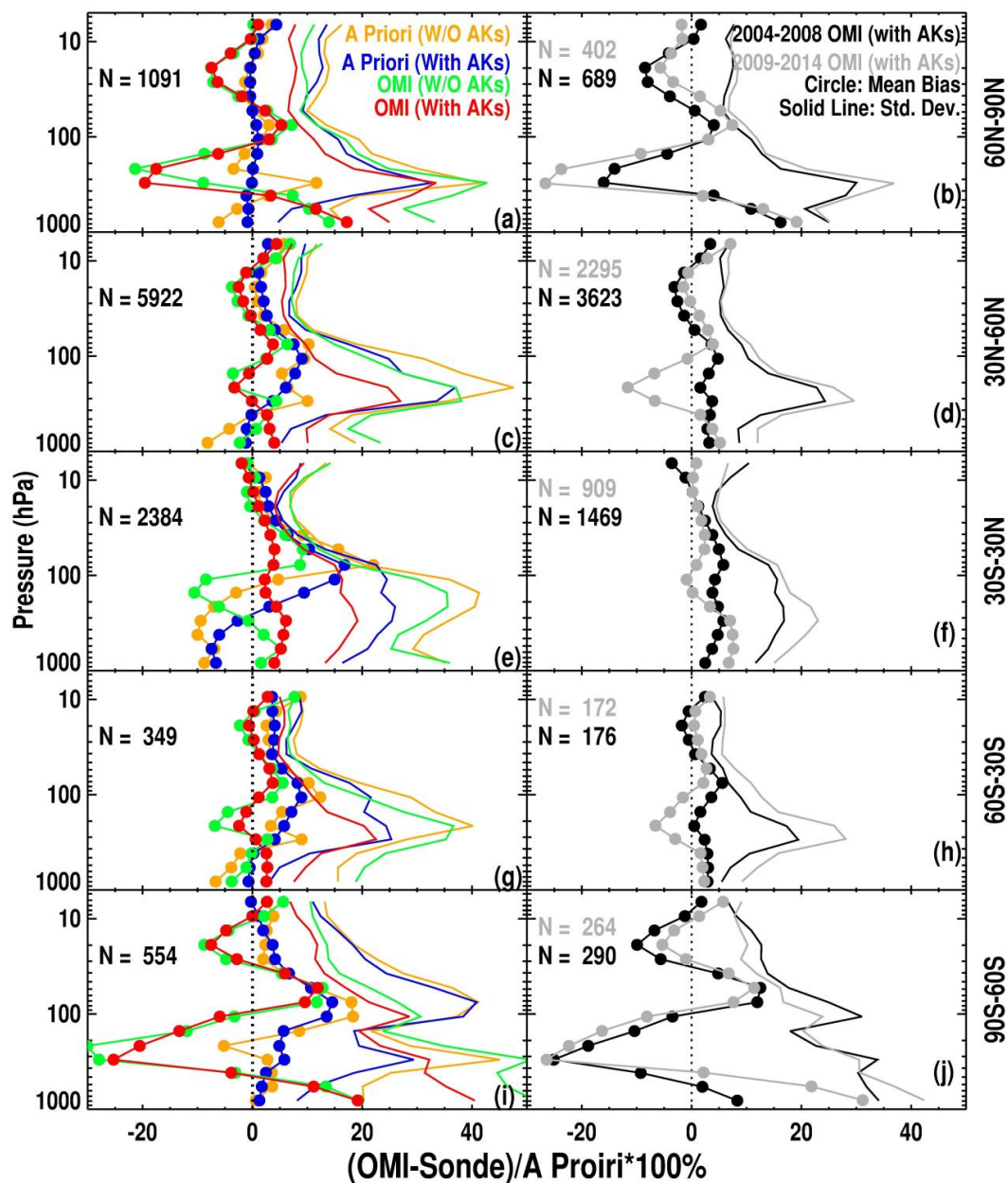
922



923

924 **Figure 2** The distribution of ozonesonde stations in this study. The color represents the mean biases
925 between OMI and ozonesonde tropospheric ozone columns (TOCs) at each station (if the number of
926 OMI and ozonesonde pairs is more than 10), and the dot size represents the standard deviation.

927



928

929 **Figure 3** Mean relative biases in ozone (line with circles) and corresponding standard deviations
 930 (solid lines) between OMI retrieval/a priori and ozonesondes with and without applying OMI
 931 retrieval averaging kernels (i.e., with AKs, and W/O AKs in red and green for comparing retrievals
 932 and in blue and yellow for comparing a priori) for five different latitude bands. The left panels show
 933 the comparison using 10 years of OMI data (2004-2014), and the right panels show the comparison

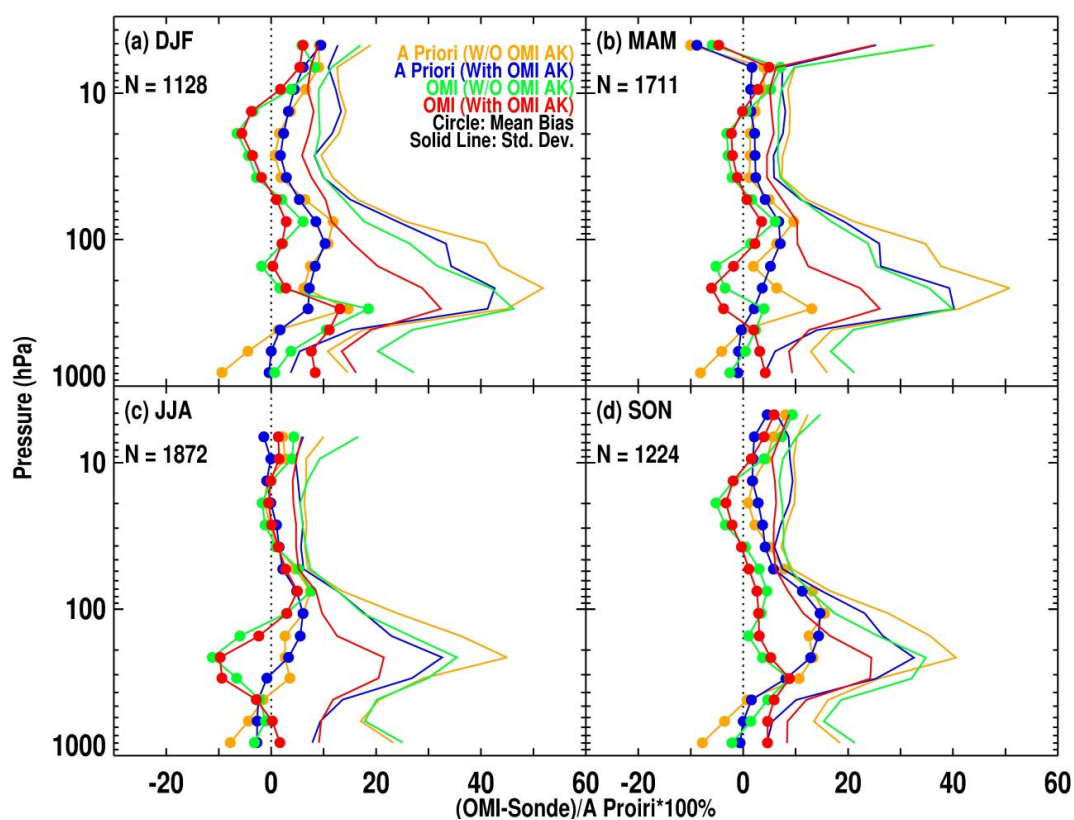


934 **between OMI retrieval and ozonesonde with OMI AKs for before and after the occurrence of serious**
935 **OMI row anomaly (RA), i.e., pre-RA (2004-2008) in black and post-RA (2009-2014) in gray,**
936 **respectively. The number (N) of OMI/ozonesonde coincidences used in the comparison is indicated**
937 **in the legends.**

938



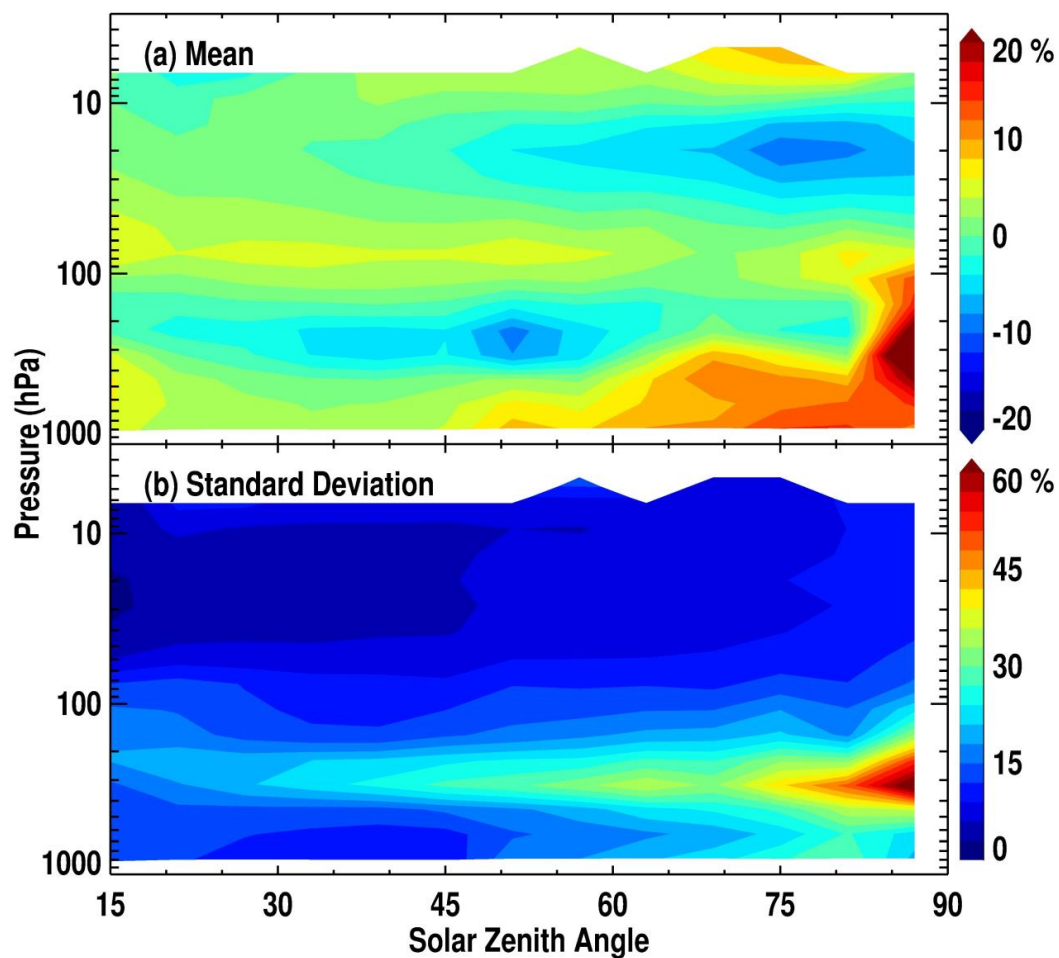
939



940

941 Figure 4 Same as Figure 3c but for each individual season at 30° N-60° N.

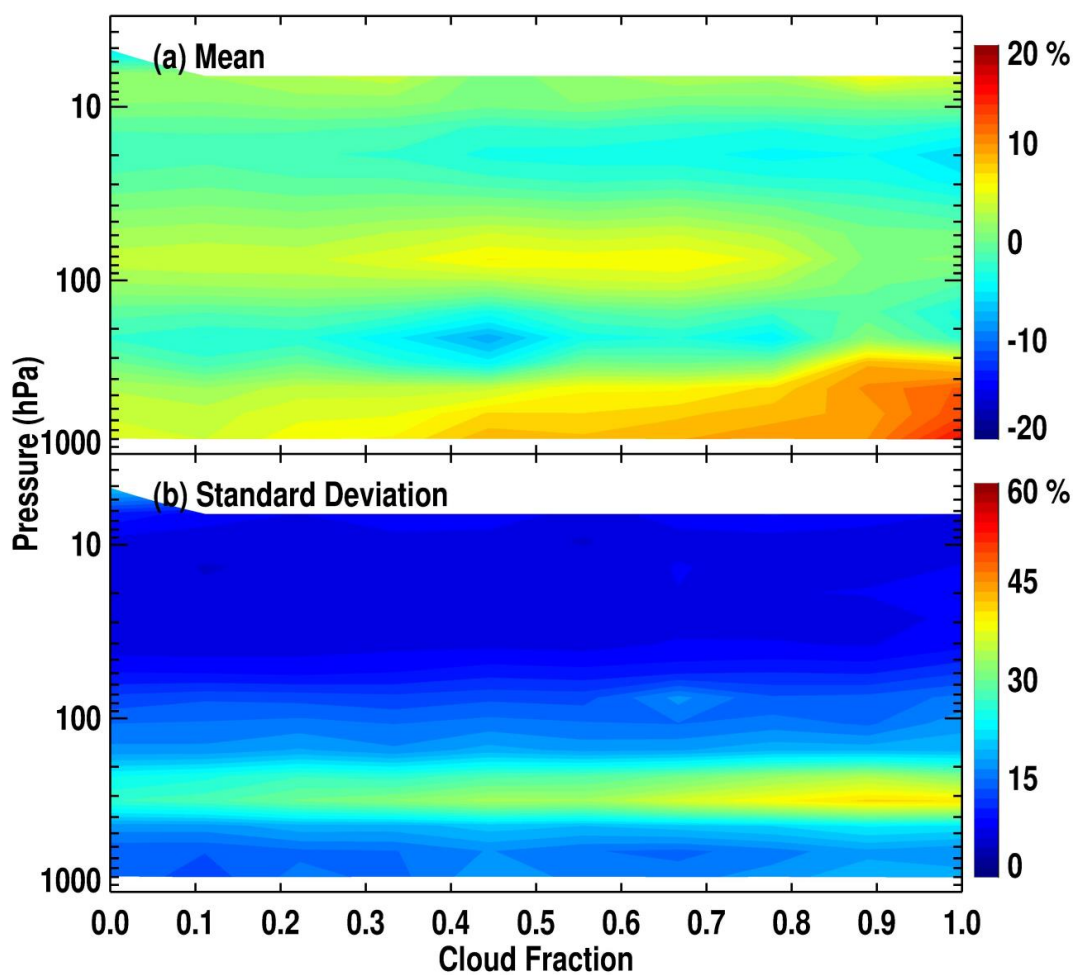
942



943

944 **Figure 5 Mean relative biases in ozone (a) and standard deviations (b) of the differences between**
945 **OMI and ozonesonde convolved with OMI AKs as a function of Solar Zenith Angle using all**
946 **OMI/ozonesonde coincidences during 2004-2014.**

947



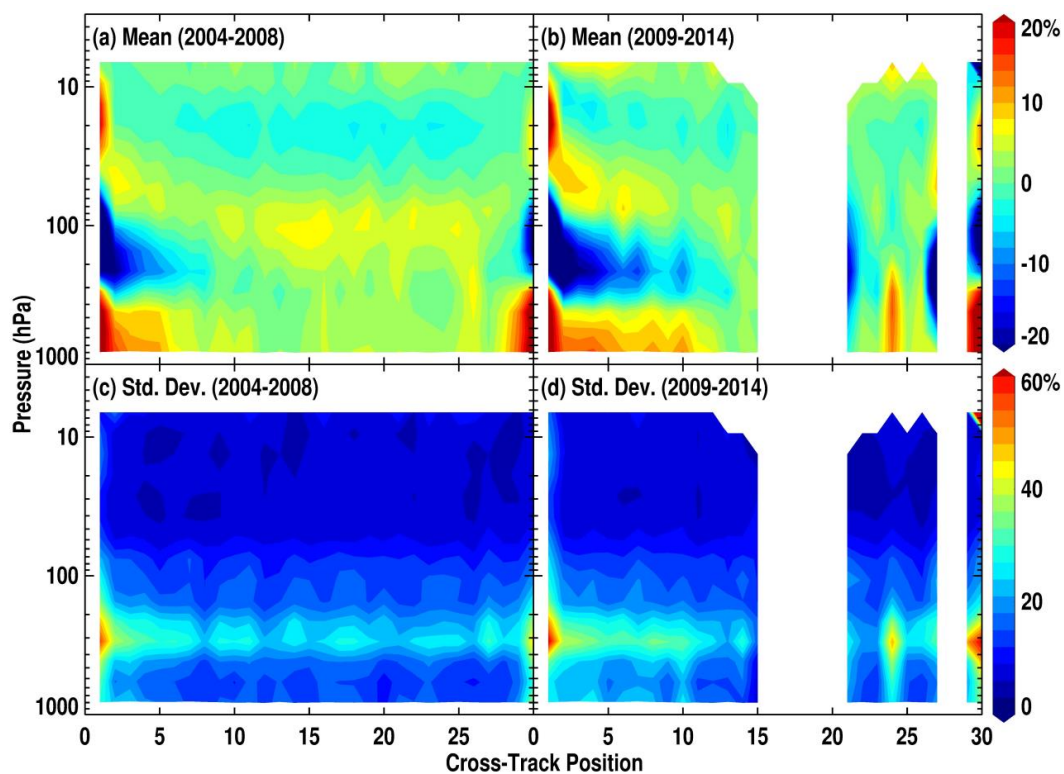
948

949 **Figure 6** Same as Figure 5 but as a function of cloud fraction.

950



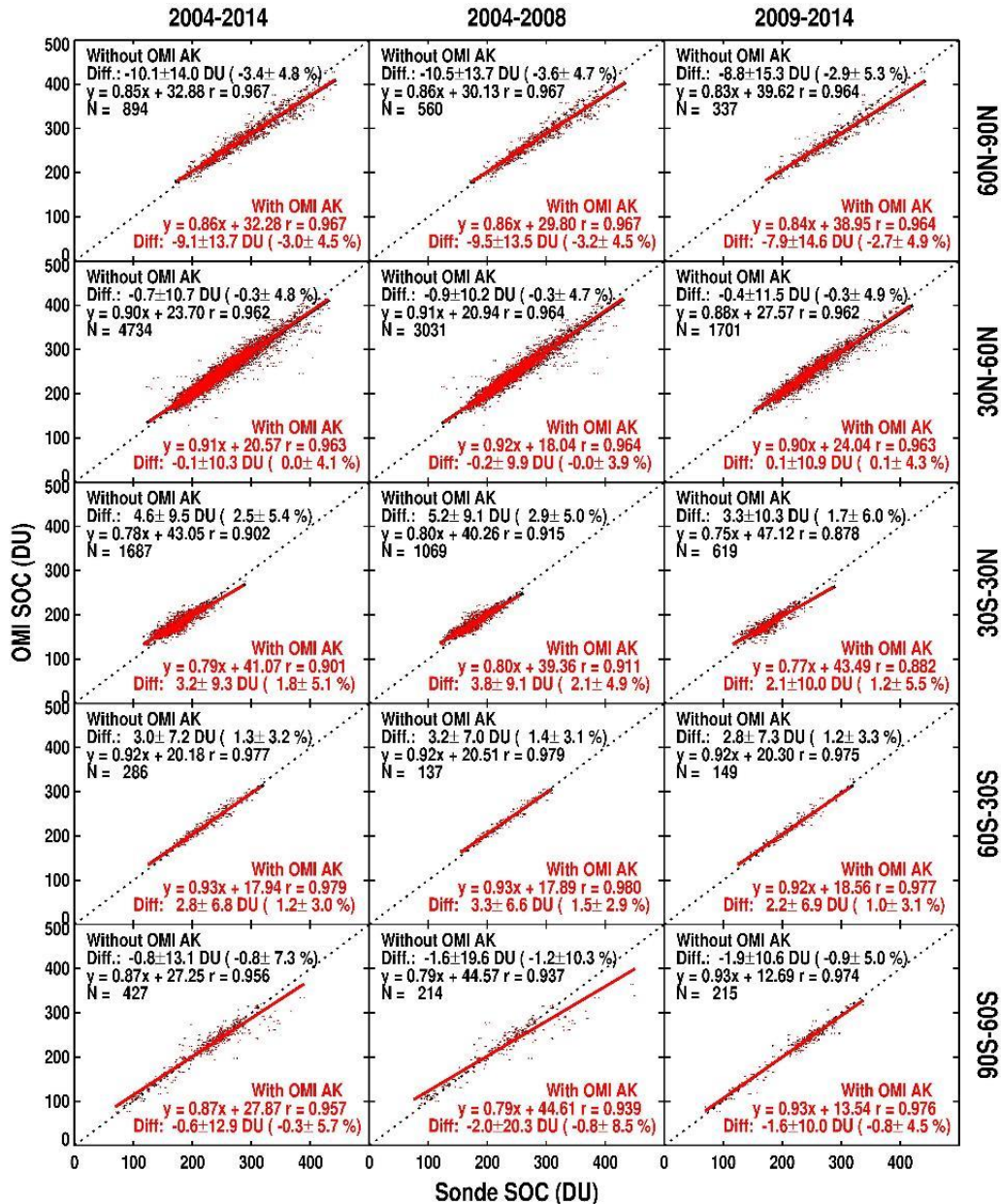
951



952

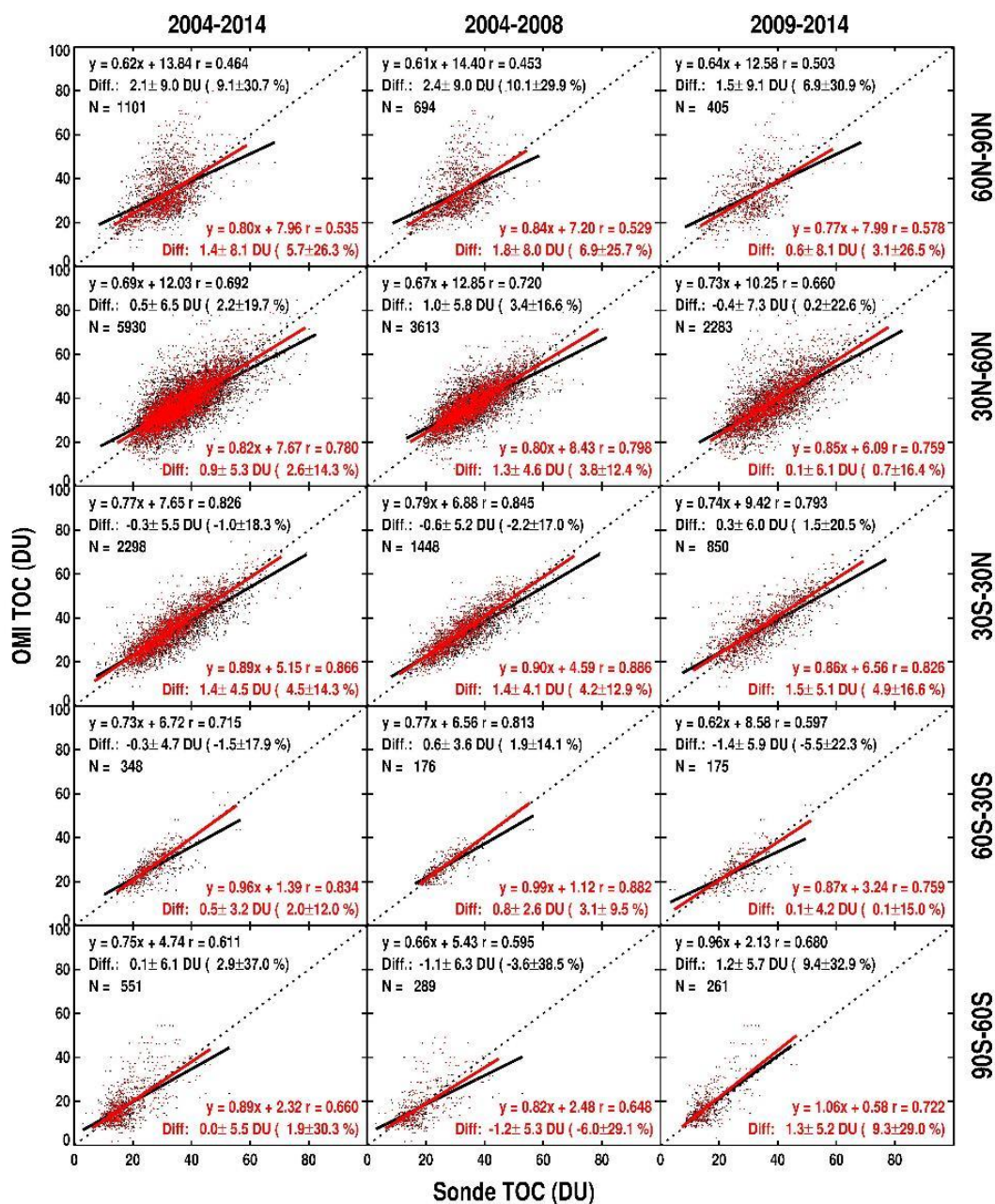
953 **Figure 7** Same as **Figure 5** but as a function of cross-track position for (left) pre-RA (2004-2008) and
954 (right) post-RA (2009-2014) periods, respectively.

955



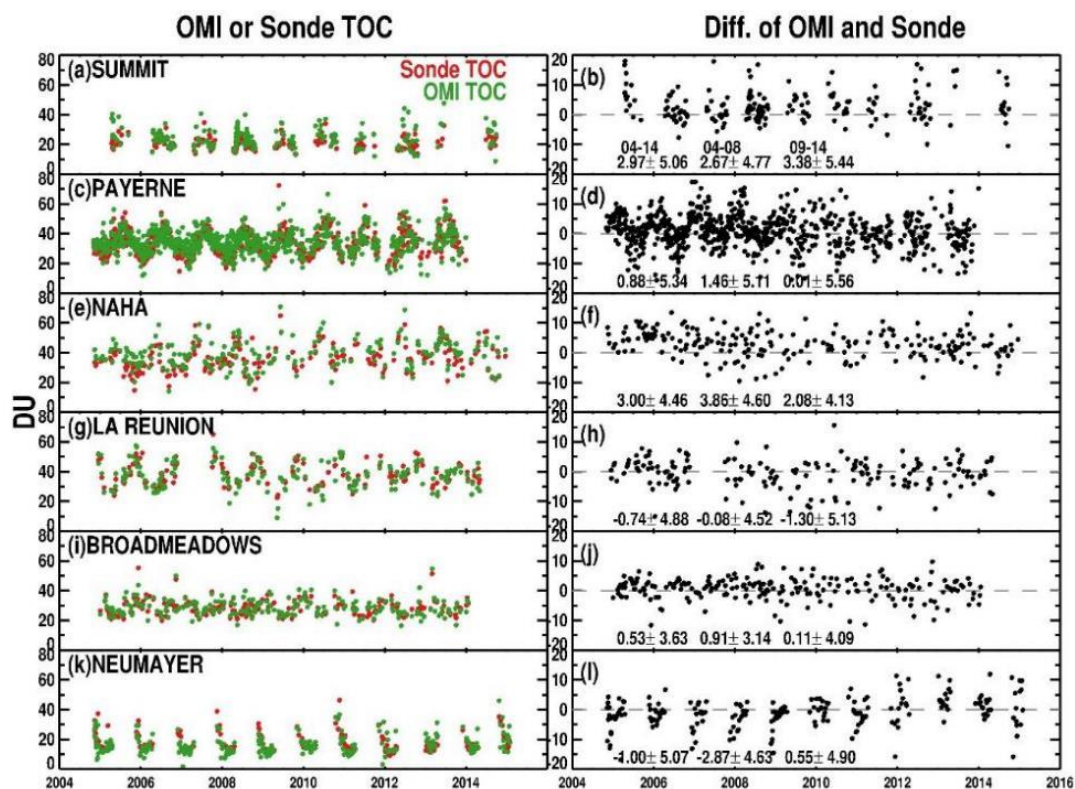
956

957 **Figure 8.** Scattering plots of OMI Stratospheric Ozone Columns (SOCs) vs. ozonesonde SOC (DU) without (black) and with (red) average kernels for five different latitude bands during 2004-2014
 958 without (black) and with (red) average kernels for five different latitude bands during 2004-2014
 959 (left), the pre-row anomaly (RA) period (i.e., 2004-2008, middle) and the post-RA period (i.e., 2009-
 960 2014, right), respectively. Comparison statistics including mean biases and standard deviations in
 961 both DU and %, the linear regression and correlation coefficients in DU, and the number of
 962 coincidences are shown in the legends.



963

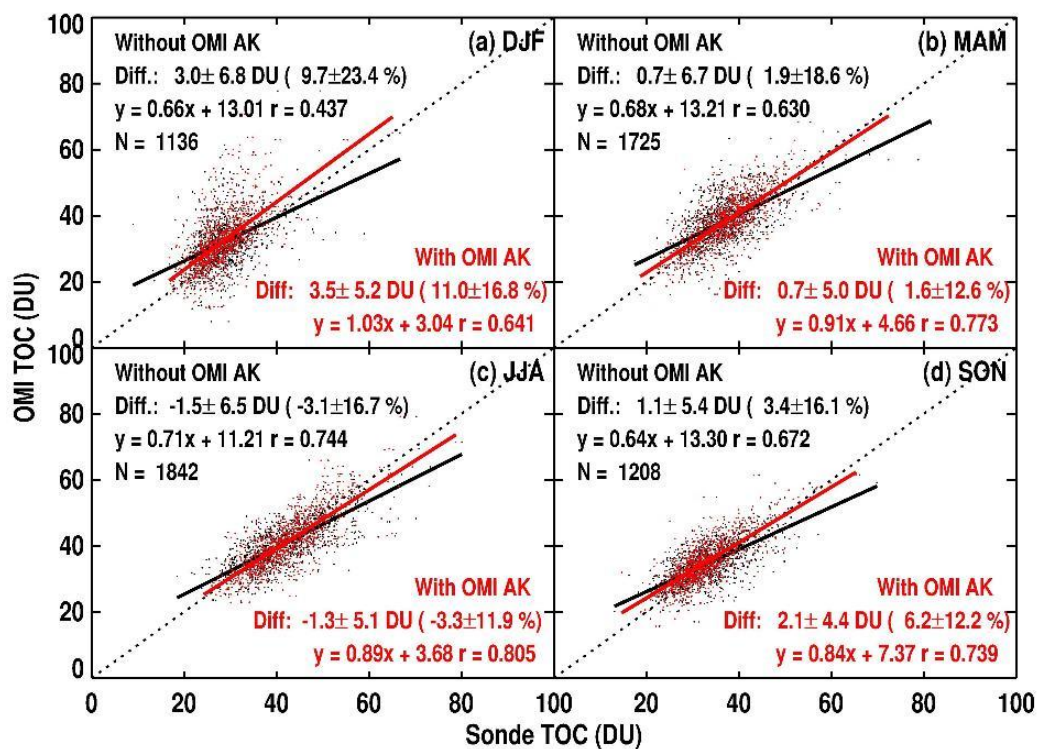
964 Figure 9. Similar to Figure 8, but for comparison of Tropospheric Ozone Columns (TOCs).



965

966 **Figure 10.** (Left) Time series of OMI tropospheric ozone columns (TOCs) as green dots and
 967 ozonesonde TOCs (with OMI AKs applied) in Summit (38.48° W, 72.57° N), Payene (6.57° E, 46.49°
 968 N), Naha (127.69° E, 26.21° N), La Réunion (55.48° E, 21.06° S), Broadmeadows (144.95° E, 58.74°
 969 S) and Neumayer (8.27° W, 70.68° S), and (Right) their corresponding differences, including the
 970 mean biases and standard deviations in 2004-2014, pre-RA (2004-2008) and post-RA (2009-2014)
 971 periods, respectively, in the legends.

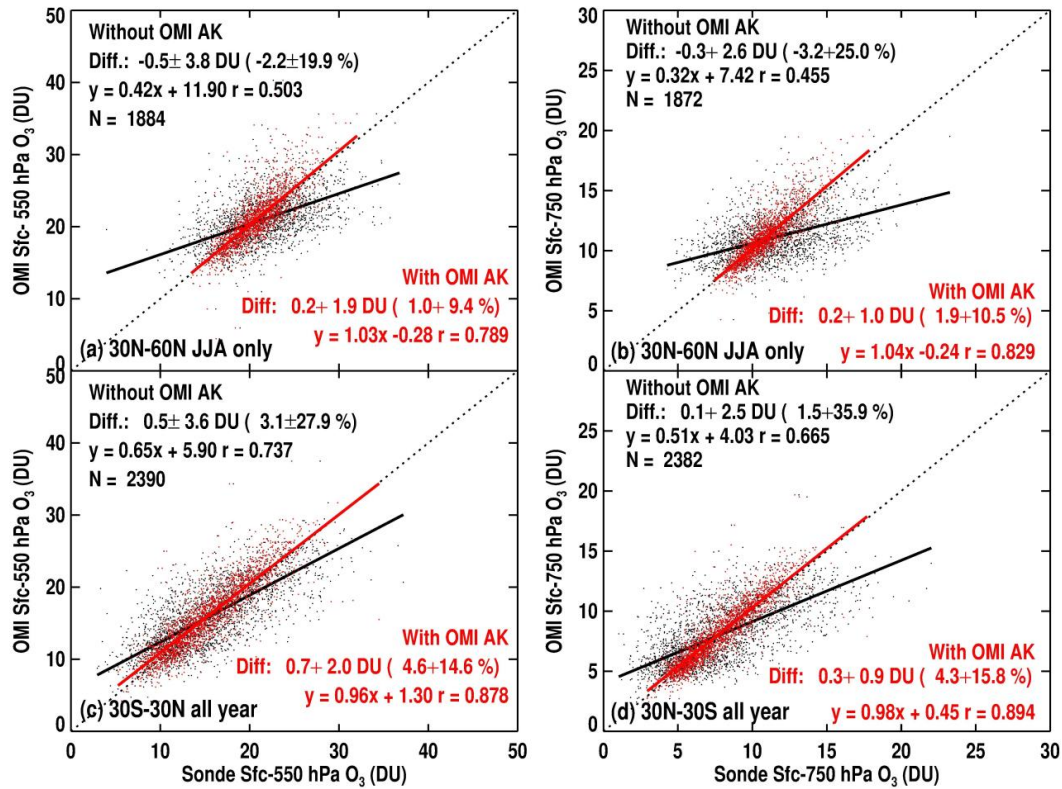
972



973

974 **Figure 11. Same as Figure 9 but for different seasons at northern middle latitude during the 2004-**
 975 **2014 period.**

976

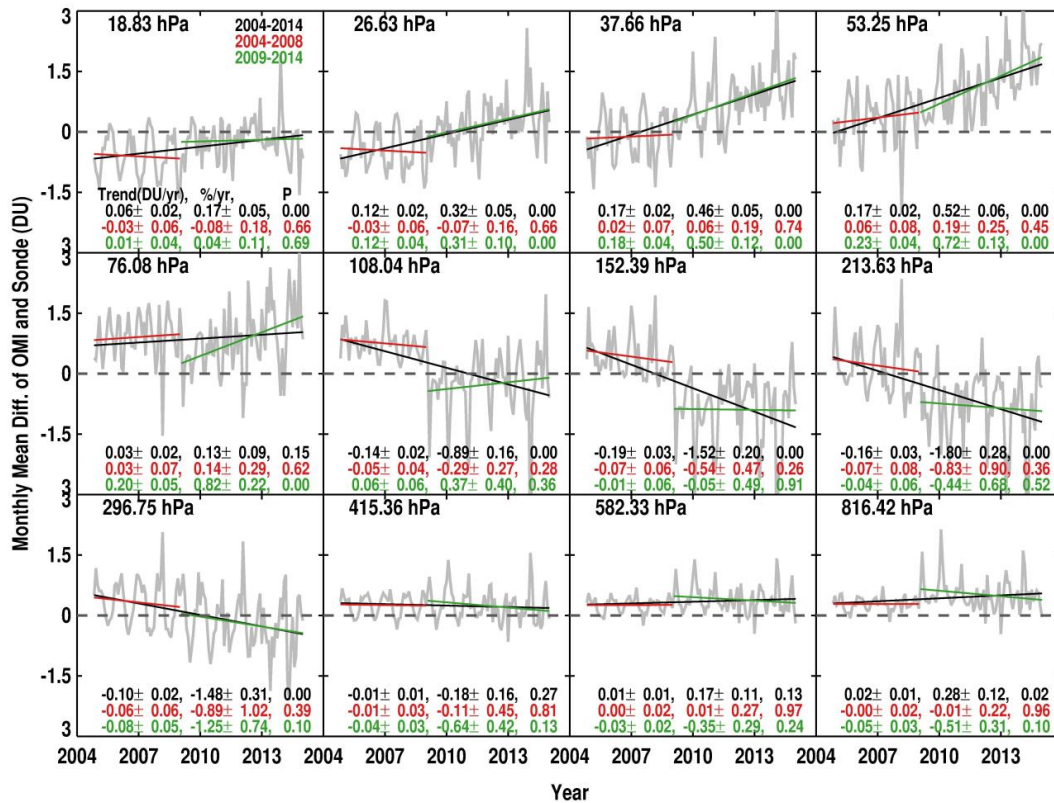


977

978 Figure 12. Same as Figure 8 but for comparison of lower tropospheric ozone columns. (a)
 979 Surface~550 hPa ozone column and (b) Surface~750 hPa ozone column in 30° N-60° N during the
 980 summer, (c) and (d) same as (a) and (b) but for the tropics.



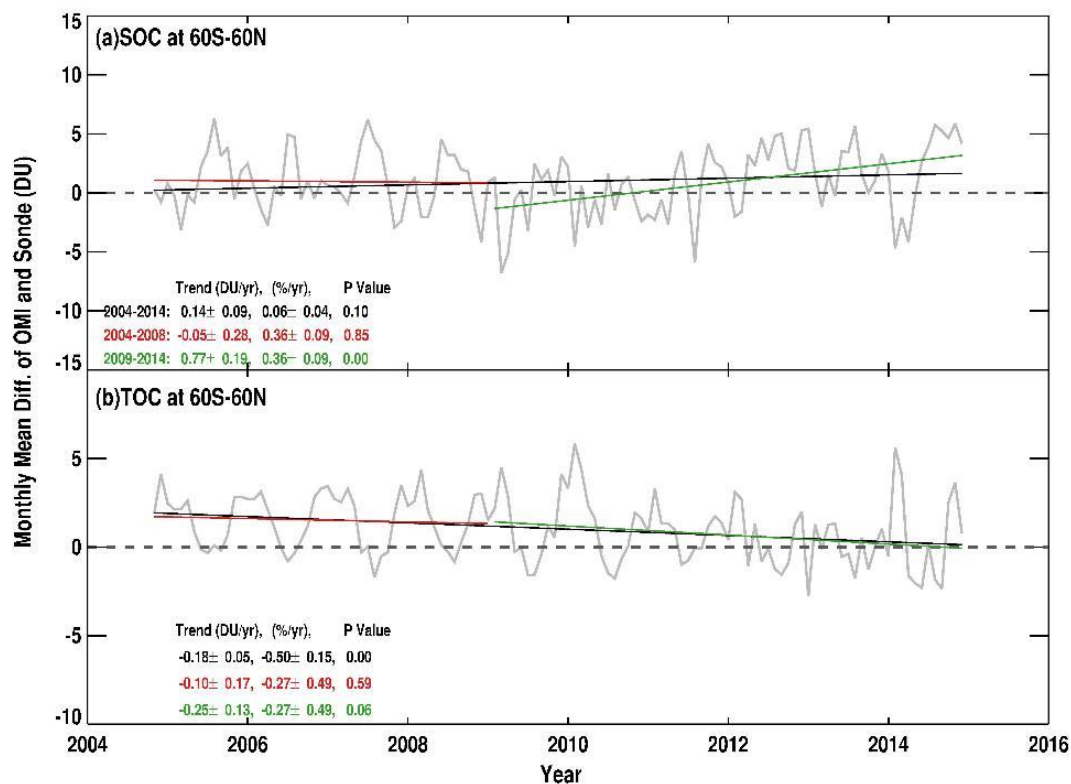
981



982

983 **Figure 13. Monthly mean variation of OMI and ozonesonde mean biases in 60° N-60° S at each OMI**
 984 **layer. The black, red and green lines represent the linear ozone bias trends in 2004-2014, pre-RA**
 985 **(2004-2008) and post-RA (2009-2014), respectively. The average altitude of each layer is marked on**
 986 **the left corner of each grid. The trends in DU/yr or % yr and P value for each time period are**
 987 **indicated in the legends.**

988



989

990 **Figure 14.** Same as Figure 13 but for Stratospheric Ozone Columns (SOCs) and Tropospheric Ozone
 991 Columns (TOCs).